Few-body approach to the structure of $\bar{K}$-nuclear quasibound states

Shota Ohnishi,[1] Wataru Horiuchi,[1] Tsubasa Hoshino,[1] Kenta Miyahara,[2] and Tetsuo Hyodo[3]
[1]*Department of Physics, Hokkaido University, Sapporo 060-0810, Japan*
[2]*Department of Physics, Kyoto University, Kyoto 606-8502, Japan*
[3]*Yukawa Institute for Theoretical Physics, Kyoto University, Kyoto 606-8502, Japan*
(Received 26 January 2017; published 6 June 2017)

The structure of light antikaon-nuclear quasibound states, which consist of an antikaon ($\bar{K} = K^-, \bar{K}^0$) and a few nucleons ($N = p,n$), such as $\bar{K}NN$, $\bar{K}NNN$, $\bar{K}NNNN$, and $\bar{K}NNNNNN$ systems, is studied with full three- to seven-body calculations. Employing a realistic $\bar{K}N$ potential based on the chiral SU(3) effective field theory with the SIDDHARTA constraint, we show that the central nucleon densities of these systems increase when the antikaon is injected, by about factor of 2 at maximum. The $\bar{K}NNNN$ system shows the largest central density, about 0.74 fm^{-3} even with the phenomenological $\bar{K}N$ potential, which is not as high as those suggested in previous studies with approximate treatments of the few-body systems. We find that the spin of the ground state of the $\bar{K}NNNNNN$ system depends on the strength of the $\bar{K}N$ attraction. Thus, the quantum number of the ground state can be another constraint on the $\bar{K}N$ interaction.

DOI: 10.1103/PhysRevC.95.065202

I. INTRODUCTION

In recent years, properties of the antikaon($\bar{K}$)-nuclear quasibound states, so-called kaonic nuclei, have been studied actively. Since the nominal location of the $\Lambda(1405)$ mass is slightly below the K^-p threshold [1], the $\Lambda(1405)$ is considered to be a $\bar{K}N$ quasibound state embedded in the $\pi\Sigma$ continuum [2,3]. Motivated by such a picture, phenomenological $\bar{K}N$ interaction models were constructed so that they reproduce the $\Lambda(1405)$ nominal mass together with two-body scattering data [4,5]. The strong attraction of the phenomenological potential models predicts deeply bound $\bar{K}$ states in light nuclei with binding energy larger than 100 MeV, and extremely dense systems about ten times higher than the ordinary nuclear density [4,6–8]. It should, however, be noted that the few-body problem was not accurately solved to predict such high-density systems, but the optical potential model or the g-matrix approach were adopted. The validity of those approaches should be examined with care, at least in the few-body systems.

The $\bar{K}N$ interactions are essential for determining the structure of the kaonic nuclei. The $\bar{K}$ belongs to a part of the pseudoscalar octet of Nambu-Goldstone bosons associated with the spontaneous symmetry breaking of chiral $SU(3)_L \times SU(3)_R$ in low-energy QCD. Thus, the chiral SU(3) effective field theory based on the symmetry breaking mechanism is a more systematic framework to obtain the $\bar{K}N$ interaction, and has succeeded in dealing with the $\bar{K}N$ interaction with $\bar{K}N$-$\pi\Sigma$ couplings [9–12]. In fact, including the next-to-leading order (NLO) contributions, the chiral SU(3) approach reproduces all existing experimental data at the level of $\chi^2/\text{d.o.f} \sim 1$ [13,14]. Among others, the precise measurement of kaonic hydrogen by the SIDDHARTA Collaboration [15,16] gives a strong constraint at the $\bar{K}N$ threshold, with which the uncertainty in the subthreshold extrapolation of the $\bar{K}N$ amplitude is significantly reduced. The equivalent single-channel $\bar{K}N$ potential to the NLO chiral dynamics including the SIDDHARTA constraint is constructed in Ref. [17] based on the framework presented in Ref. [18]. Thus, the realistic $\bar{K}N$ potential is now available.

The $\bar{K}N$-$\pi\Sigma$ scattering amplitude from the chiral SU(3) dynamics has two poles in the $\Lambda(1405)$ energy region [11,19,20]: one is located around 1420 MeV, while the other exhibits a broad resonant structure above the $\pi\Sigma$ threshold. The pole located around 1420 MeV corresponds to the $\bar{K}N$ quasibound state with a binding energy of 15 MeV, about a half of the binding energy assumed in the phenomenological $\bar{K}N$ interactions. This different pole structure comes from different off-shell properties of the $\bar{K}N$ interactions. The $\bar{K}N$ interaction based on the chiral SU(3) dynamics is energy dependent, and that in the subthreshold becomes less attractive than the one proposed by the energy-independent phenomenological potential [18]. These different off-shell properties also appear in how the $\Lambda(1405)$ resonance shows up in the differential cross section of the $K^-d \to \pi\Sigma n$ reaction [21]. These differences are further enhanced in the light kaonic nuclei. For the lightest kaonic nuclei, so-called strange dibaryons in the $\bar{K}NN$-πYN ($Y = \Sigma, \Lambda$) coupled system, the energy-dependent potential models [22–26] give resonance energies higher than the energy-independent ones [6,27–32]. How a possible signature of this strange dibaryon resonance shows up in the resonance production reaction is also of interest, as it reflects the two-body dynamics of the $\bar{K}N$ system [33].

Given the background described above, we raise three questions to be discussed in this paper: (1) What are the structures of light kaonic nuclei when reliable NN and $\bar{K}N$ interactions are used? (2) Can the high-density $\bar{K}$ nuclei be realized within the accurate few-body treatment? (3) How does the off-shell dependence of the $\bar{K}N$ interaction affect few-body systems? To answer these questions, we perform fully microscopic few-body calculations for three- to seven-body systems including an antikaon. Here, the systems with a $\bar{K}$ and $(\mathcal{N}-1)$ nucleons are accurately described by employing the stochastic variational method (SVM) with correlated Gaussian (CG) basis [34–36]. We employ the $\bar{K}N$ interaction based on the chiral SU(3) dynamics with the SIDDHARTA constraint [17] as a realistic $\bar{K}N$ force. Combining them with the reliable nuclear forces, we present quantitative predictions

 ©2017 American Physical Society

of the structure of the light kaonic nuclei. Next, we perform the same few-body calculations with the phenomenological $\bar{K}N$ interaction, the so-called Akaishi-Yamazaki (AY) potential [4,27], in order to examine the validity of the many-body approximations used in the prediction of the high-density states. Furthermore, the comparison of the results with two $\bar{K}N$ potentials serves as a study of the off-shell dependence of the interactions. In this way, we systematically study the structure of kaonic nuclei and discuss how the nuclear structure is changed by $\bar{K}$.

In Sec. II, we briefly review the two-body interactions used in this work. The SVM with the CG basis for the $\mathcal{N}$-body systems is explained in Sec. III. We summarize the quantities to analyze the structures of the few-body systems in Sec. IV. Numerical results of the properties of the light kaonic nuclei are presented in Sec. V. A summary is given in Sec. VI.

II. TWO-BODY INTERACTIONS

A. Hamiltonian and expectation values

The Hamiltonian for $(\mathcal{N}-1)$ nucleons and an antikaon takes the form

$$H = \sum_{i=1}^{\mathcal{N}} T_i - T_{\rm cm} + \sum_{i<j}^{\mathcal{N}-1} V_{ij}^{(NN)} + \sum_{i=1}^{\mathcal{N}-1} V_{i\mathcal{N}}^{(\bar{K}N)} + \sum_{i<j}^{\mathcal{N}} V_{ij}^{\rm Coul.}. \quad (1)$$

Here T_i is the kinetic energy of the ith particle. The particle label, $i=\mathcal{N}$, always indicates an antikaon and the others are for nucleons. $T_{\rm cm}$ is the energy of the center-of-mass (c.m.) motion,

$$T_{\rm cm} = \frac{\left(\sum_{i=1}^{\mathcal{N}} \boldsymbol{p}_i\right)^2}{2\{(\mathcal{N}-1)m_N + m_{\bar{K}}\}}, \quad (2)$$

where the isospin-averaged nucleon and antikaon masses, $m_N = 939$ MeV and $m_{\bar{K}} = 496$ MeV, are used in this paper. $V_{ij}^{(NN)}$, $V_{ij}^{(\bar{K}N)}$, and $V_{ij}^{\rm Coul.}$ are the NN, $\bar{K}N$, and Coulomb interactions between the ith and jth particles, respectively. The NN and $\bar{K}N$ interactions depend on isospin of two-particles, and they can be written as

$$V_{ij} = V_{ij}^{I=0}\hat{P}_{ij}^{I=0} + V_{ij}^{I=1}\hat{P}_{ij}^{I=1} = \tfrac{1}{2}\left(V_{ij}^{I=0} + V_{ij}^{I=1}\right) - \tfrac{1}{2}\left(V_{ij}^{I=0} - V_{ij}^{I=1}\right)\hat{P}_{\tau}^{ij}, \quad (3)$$

where $\hat{P}_{ij}^{I=0} = \frac{1-\boldsymbol{\tau}_i\cdot\boldsymbol{\tau}_j}{4}$ and $\hat{P}_{ij}^{I=1} = \frac{3+\boldsymbol{\tau}_i\cdot\boldsymbol{\tau}_j}{4}$ are isospin-projection operators for $I=0$ and 1, and $\hat{P}_{\tau}^{ij} = \frac{1+\boldsymbol{\tau}_i\cdot\boldsymbol{\tau}_j}{2}$ is the isospin-exchange operator for the ith and jth particles. The isospin-exchange operator $\hat{P}_\tau$ acts on the particle basis as $\hat{P}_\tau|nn\rangle = |nn\rangle$, $\hat{P}_\tau|pp\rangle = |pp\rangle$ and $\hat{P}_\tau|pn\rangle = |np\rangle$ for NN, and $\hat{P}_\tau|K^-n\rangle = |K^-n\rangle$, $\hat{P}_\tau|\bar{K}^0p\rangle = |\bar{K}^0p\rangle$, $\hat{P}_\tau|K^-p\rangle = -|\bar{K}^0n\rangle$ and $\hat{P}_\tau|\bar{K}^0n\rangle = -|K^-p\rangle$ for $\bar{K}N$. We have to treat the K^-p-$\bar{K}^0n$ channel coupling explicitly in the particle basis calculation.

The single-channel $\bar{K}N$ potential $V^{(\bar{K}N)}$ has an imaginary part which represents the decay processes into the lower energy $\pi\Sigma$ and $\pi\Lambda$ channels. Because of the complex nature of the potential, the Hamiltonian is non-Hermite and can have an eigenstate with a complex eigenvalue, called a quasibound state. In order to discuss the structure of the quasibound state, we need to evaluate the expectation values of some operators. For a stable bound state, the expectation value of an operator $\hat{\mathcal{O}}(\boldsymbol{x})$ with the wave function $\Psi_{JMM_T}(\boldsymbol{x})$ is given by (notation of the wave function will be explained in Sec. III)

$$\langle\hat{\mathcal{O}}\rangle \equiv \int d\boldsymbol{x}\left[\Psi_{JMM_T}(\boldsymbol{x})\right]^*\hat{\mathcal{O}}(\boldsymbol{x})\Psi_{JMM_T}(\boldsymbol{x}) \quad (4)$$

with the normalization of the wave function

$$1 = \int d\boldsymbol{x}\left|\Psi_{JMM_T}(\boldsymbol{x})\right|^2. \quad (5)$$

However, since the eigenfunctions of a non-Hermite Hamiltonian do not form an orthogonal set [37], we should introduce the Gamow states to treat an unstable state. The expectation value with the Gamow states is

$$\langle\hat{\mathcal{O}}\rangle_G \equiv \int d\boldsymbol{x}\,\Psi_{JMM_T,G}(\boldsymbol{x})\hat{\mathcal{O}}(\boldsymbol{x})\Psi_{JMM_T,G}(\boldsymbol{x}) \quad (6)$$

with the normalization

$$1 = \int d\boldsymbol{x}\left[\Psi_{JMM_T,G}(\boldsymbol{x})\right]^2. \quad (7)$$

With the normalization of Eq. (7), expectation values are in general obtained as complex numbers, which are not straightforwardly interpreted. In some cases, however, we can extract a real-valued quantity. As explained in the Appendix of Ref. [17], for a quasibound state whose real part of the eigenenergy is negative, the damping of the wave function outside the potential can be extracted from the standard expectation values with the normalization (4). In this paper, we calculate the root-mean-square (rms) distances $\sqrt{\langle r^2\rangle}$, density distributions $\rho(r)$, and the probabilities of finding various channels in the wave functions P by using the standard expectation value (4). For the other operators such as Hamiltonian and its decomposition, the expectation values are calculated by using Gamow state normalization (7).

B. NN interactions

As a nucleon-nucleon interaction $V^{(NN)}$ we employ the Argonne V4′ potential [38]. The AV4′ potential is obtained by simplifying the full AV18 potential by suppressing the small electromagnetic, the spin-orbit, and the tensor terms and readjusting the central spin- and isospin-dependent interactions. Table I lists the binding energies and radii of two- to six-nucleon systems calculated with the AV4′ potential. The AV4′ potential model reasonably reproduces the properties of light nuclei.

C. $\bar{K}N$ interactions

As a realistic $\bar{K}N$ interaction, $V^{(\bar{K}N)}$, we employ the Kyoto $\bar{K}N$ potential, which is the energy-dependent effective interaction based on the chiral SU(3) dynamics constructed in

TABLE I. Total binding energies B, point-proton rms radii $\sqrt{\langle r_p^2\rangle}$, point-neutron rms radii $\sqrt{\langle r_n^2\rangle}$ and rms matter radii $\sqrt{\langle r_N^2\rangle}$ of ordinary nuclei. The experimental data of the binding energies B are taken from Ref. [39]. The nuclear charge radii $\sqrt{\langle r_{ch}^2\rangle}$ in Ref. [40] are converted into point-proton rms radii $\sqrt{\langle r_p^2\rangle}$ by using the formula: $\langle r_{ch}^2\rangle = \langle r_p^2\rangle + \langle r_{pc}^2\rangle + \frac{N}{Z}\langle r_{nc}^2\rangle + \frac{3}{4m_p^2}$ [41], where $\langle r_{pc}^2\rangle = 0.878^2$ fm^2, $\langle r_{nc}^2\rangle = -0.115$ fm^2, and $\frac{3}{4m_p^2} = 0.0332$ fm^2 are proton mean-square charge radius, neutron mean-square charge radius, and Darwin-Foldy term, respectively.

	AV4′	Expt.	AV4′	Expt.	AV4′	
	B (MeV)		$\sqrt{\langle r_p^2\rangle}$ (fm)		$\sqrt{\langle r_n^2\rangle}$ (fm)	$\sqrt{\langle r_N^2\rangle}$ (fm)
^{2}H	2.24	2.22	2.02	1.97	2.02	2.02
^{3}H	8.99	8.48	1.59	1.59	1.70	1.67
^{3}He	8.33	7.72	1.73	1.77	1.60	1.69
^{4}He	32.1	28.3	1.39	1.46	1.38	1.39
^{6}He	32.2	29.3	2.00	1.93	2.95	2.67
^{6}Li	35.8	32.0	2.43	2.45	2.42	2.43

Ref. [17]:

$$V^{(\bar{K}N)}(r,E) = \frac{1}{\pi^{3/2}b^3}e^{-r^2/b^2}\frac{m_N}{2(E+m_N+m_{\bar{K}})} \times \frac{\omega_{\bar{K}}+E_N}{\omega_{\bar{K}}E_N}\left[\sum_{i=0}^{10}K_i\left(\frac{E}{100\ \text{MeV}}\right)^i\right], \quad (8)$$

where E, E_N, and $\omega_{\bar{K}}$ are the nonrelativistic two-body energy, the energy of the nucleon and the energy of the antikaon:

$$E = \sqrt{s} - m_N - m_{\bar{K}}, \quad (9)$$

$$E_N = \frac{s - m_{\bar{K}}^2 + m_N^2}{2\sqrt{s}}, \quad (10)$$

$$\omega_{\bar{K}} = \frac{s - m_N^2 + m_{\bar{K}}^2}{2\sqrt{s}}. \quad (11)$$

The coefficients K_i of the energy-dependent strength and the range parameter b are determined so as to reproduce the $\bar{K}N$ amplitude [13,14] calculated based on the NLO chiral SU(3) dynamics (see Ref. [17]). The Kyoto $\bar{K}N$ potential is the single channel $\bar{K}N$ interaction model where the meson-baryon channel coupling effect with strangeness $S=-1$ is renormalized, and thus the coefficients K_i are the complex numbers. The origin of the energy dependence is twofold. The coupled-channel interaction depends on the energy through the time derivatives in the chiral Lagrangians, and the construction of the equivalent single-channel potential introduces additional energy dependence. By solving the Schrödinger equation, the pole positions of the $\bar{K}N(I=0)$ amplitude are found to be $1424-26i$ and $1381-81i$ MeV.

For the use of the energy-dependent potential, it is necessary to determine the $\bar{K}N$ two-body energies in the $\mathcal{N}$-body systems. Though the two-body energies in the $\mathcal{N}$-body systems cannot be determined uniquely, we follow the same way as used in Refs. [22,23] to determine the $\bar{K}N$ two-body energies for practical calculations.[1] First, we introduce an "antikaon binding energy" $B_{\bar{K}}$ as

$$-B_{\bar{K}} \equiv \langle H\rangle_G - \langle H_N\rangle_G, \quad (12)$$

where H_N is the Hamiltonian for $(\mathcal{N}-1)$ nucleons defined by

$$H_N = \sum_{i=1}^{\mathcal{N}-1}T_i - T_{\text{cm}}^N + \sum_{i<j}^{\mathcal{N}-1}V_{ij}^{(NN)} + \sum_{i<j}^{\mathcal{N}-1}V_{ij}^{\text{Coul.}} \quad (13)$$

with

$$T_{\text{cm}}^N = \frac{\left(\sum_i^{\mathcal{N}-1}\boldsymbol{p}_i\right)^2}{2(\mathcal{N}-1)m_N}. \quad (14)$$

Note that $-B_{\bar{K}}$ is in general complex. We employ the following three types of the $\bar{K}N$ two-body energy:

$$\sqrt{s} = m_N + m_{\bar{K}} + \delta\sqrt{s}, \quad (15)$$

$$\text{Type I:}\quad \delta\sqrt{s} = -B_{\bar{K}}, \quad (16)$$

$$\text{Type II:}\quad \delta\sqrt{s} = -B_{\bar{K}}/(\mathcal{N}-1). \quad (17)$$

Type I corresponds to the picture in which the $\bar{K}$ field collectively surrounds the $(\mathcal{N}-1)$ nucleons, and Type II corresponds to the picture in which the $\bar{K}$ energy is distributed equally to the $(\mathcal{N}-1)$ nucleons [22,23]. The eigenstate is determined in a self-consistent manner; the two-body energy calculated by the expectation values in Eq. (15) should equal to the energy variable in the $\bar{K}N$ interaction in $V^{(\bar{K}N)}(r,E)$.

For comparison, we also examine the Akaishi-Yamazaki (AY) potential. The potential was originally constructed in the coupled-channel $\bar{K}N$-$\pi\Sigma$-$\pi\Lambda$ system by fitting the old data of the scattering lengths in Ref. [42] and the nominal pole position of $\Lambda(1405)$ [4]. Here we adopt the single-channel version presented in Ref. [27] in which the energy dependence of the potential through the Feshbach projection method is eliminated by hand.

We note that the imaginary parts of the Kyoto $\bar{K}N$ and AY potentials represent the decay into the $\pi\Sigma$ and $\pi\Lambda$ channels. In the few-body kaonic nuclei, there are two types of the decay processes: the mesonic decays with a pion emission and the nonmesonic decays with multinucleon absorptions. In this work, the imaginary part of the eigenenergy corresponds only to the mesonic decay width, reflecting the imaginary part of the two-body potential. When the nonmesonic decays are taken into account, they increase the decay width of the kaonic nuclei by several tens of MeV [23,43–45].

III. STOCHASTIC VARIATIONAL METHOD WITH CORRELATED GAUSSIAN BASIS

We investigate the structure of the kaonic nuclei with a powerful few-body approach, that is, the SVM with the CG basis [34–36]. The method is flexible to cope with strongly

[1] We also examine the prescription of the two-body energy suggested in Ref. [25]. The results of the few-body systems turn out to be in between the two choices shown in this paper.

correlated few-particle quantum systems as exemplified in Ref. [46].

The wave function for the $\mathcal{N}$-body system is expanded as a combination of the basis functions:

$$\Psi_{JMM_T}(\boldsymbol{x}) = \sum_{k=1}^{K} c_k \Phi_{JMM_T}(\boldsymbol{x}, A_k), \tag{18}$$

where J is the total angular momentum and M (M_T) is the z component of the total angular momentum (isospin). Since we employ central NN and $\bar{K}N$ interactions, no channel coupling occurs between states with different L. In this paper, we consider total orbital momentum $L = 0$ state by taking the basis functions with total spin $J(= S)$ to have the form

$$\Phi_{SM_SM_T}(\boldsymbol{x}, A) = \mathscr{A}\{\exp(-\tilde{\boldsymbol{x}} A \boldsymbol{x})\chi_{SM_S}\eta_{M_T}\}, \tag{19}$$

where the operator $\mathscr{A}$ is an antisymmetrizer for the nucleons; M_S $(=M)$ is the z components of the total spin; $\boldsymbol{x}$ is an $(\mathcal{N}-1)$-dimensional column vector, whose ith element is a three-dimensional Jacobi coordinate $\boldsymbol{x}_i$; the symbol $\tilde{\boldsymbol{x}}$ stands for a transpose of $\boldsymbol{x}$; A is an $(\mathcal{N}-1)\times(\mathcal{N}-1)$ positive-definite symmetric matrix. The Jacobi coordinates $\boldsymbol{x}_i$, including the center-of-mass coordinate $\boldsymbol{x}_{\mathcal{N}}$, are related to the ith single-particle coordinate $\boldsymbol{r}_i$ by a linear transformation:

$$\boldsymbol{x}_i = \sum_{j=1}^{\mathcal{N}} U_{ij}\boldsymbol{r}_j \tag{20}$$

with

$$U = \begin{pmatrix} 1 & -1 & 0 & \cdots & 0 \\ \frac{1}{2} & \frac{1}{2} & -1 & \cdots & 0 \\ \vdots & & \ddots & \ddots & \vdots \\ \frac{1}{\mathcal{N}-1} & \cdots & \cdots & \frac{1}{\mathcal{N}-1} & -1 \\ \frac{m_N}{(\mathcal{N}-1)m_N+m_{\bar{K}}} & \cdots & \cdots & \frac{m_N}{(\mathcal{N}-1)m_N+m_{\bar{K}}} & \frac{m_{\bar{K}}}{(\mathcal{N}-1)m_N+m_{\bar{K}}} \end{pmatrix}. \tag{21}$$

We can easily apply the CG to the present three- to seven-body model because the CG keeps its functional form under any linear transformation between different coordinate sets for any number of particles. The CG basis in Eq. (19) can only be applicable to states with total orbital angular momentum $L = 0$. It should be noted that the higher partial waves for each coordinate are taken into account through the cross terms, $\boldsymbol{x}_i \cdot \boldsymbol{x}_j$.

The spin wave function χ_{SM_S} is expressed using the basis of successive coupling:

$$\chi_{SM_S} = \left|\left[\cdots\left[\left[\tfrac{1}{2}\tfrac{1}{2}\right]_{S_{12}}\tfrac{1}{2}\right]_{S_{123}}\cdots\right]_{SM_S}\right\rangle. \tag{22}$$

Here we take all possible intermediate spins $(S_{12}, S_{123}, \ldots)$ for a given S. For the isospin wave function, η_{M_T}, we employ the particle basis, which is given as the product of single-particle isospin wave functions:

$$\eta_{M_T} = \eta_{\frac{1}{2}m_{\tau_1}} \cdots \eta_{\frac{1}{2}m_{\tau_{\mathcal{N}}}}. \tag{23}$$

The sets of the single-particle isospins $(m_{\tau_1}, \ldots, m_{\tau_{\mathcal{N}}})$ take the values

$$m_{\tau_k} = \begin{cases} \frac{1}{2} & (k = 1, \ldots, M_T + \frac{\mathcal{N}}{2} - 1, \mathcal{N}), \\ -\frac{1}{2} & (\text{otherwise}) \end{cases} \tag{24}$$

for the states with $\bar{K}^0$ and

$$m_{\tau_k} = \begin{cases} \frac{1}{2} & (k = 1, \ldots, M_T + \frac{\mathcal{N}}{2}), \\ -\frac{1}{2} & (\text{otherwise}) \end{cases} \tag{25}$$

for the states with K^-.

Each basis function has $\mathcal{N}(\mathcal{N}-1)/2$ nonlinear parameters $(A_k)_{ij}$ and also spin and isospin quantum numbers. The adequate choice of these parameters is crucial to determine accuracy of the variational calculation. The SVM offers efficient and economical ways to find optimal sets of the variational parameters [34–36], in which we increase the basis size one-by-one by searching for the best among many random trials for the basis function. For the Hermitian Hamiltonian, the eigenvalues for the trial wave functions are larger than or equal to the exact eigenvalue. Since we use the complex $\bar{K}N$ potential in this work, the eigenvalues of the trial wave functions give no longer the lower limit. Practically, we apply the SVM for the real part of the Hamiltonian to obtain the energy curve, and then we diagonalize the full Hamiltonian by using the basis optimized for the ground state with the real Hamiltonian. The validity of this method can be confirmed in the two-body sector where the exact value of the pole position can be obtained. Examples of the few-body calculations for $\bar{K}NN$ (K^-pp), $\bar{K}NNN$ ($^3_{\bar{K}}$H), $\bar{K}NNNN$ ($^4_{\bar{K}}$H), and $\bar{K}NNNNNN$ [$^6_{\bar{K}}$He (J^π)] are shown in Fig. 1 with the AY potential. The eigenvalues with the real part of the Hamiltonian are shown in Fig. 1(a). Corresponding complex energy curves of the full Hamiltonian are plotted in Figs. 1(b) and 1(c). We find that if the energy convergence is reached with the real part of the Hamiltonian, the eigenvalues with the full Hamiltonian are also converged. The obtained energies in this method are consistent with other calculations for two- and three-body systems [4,6,27].

For the $\bar{K}NN$, $\bar{K}NNN$, $\bar{K}NNNN$, and $\bar{K}NNNNNN$ systems, the basis sizes are 200, 1000, 4000, and 10000, respectively. The binding energies and widths change less than 0.0001 MeV when the numbers of basis increase by 1 from these basis numbers.

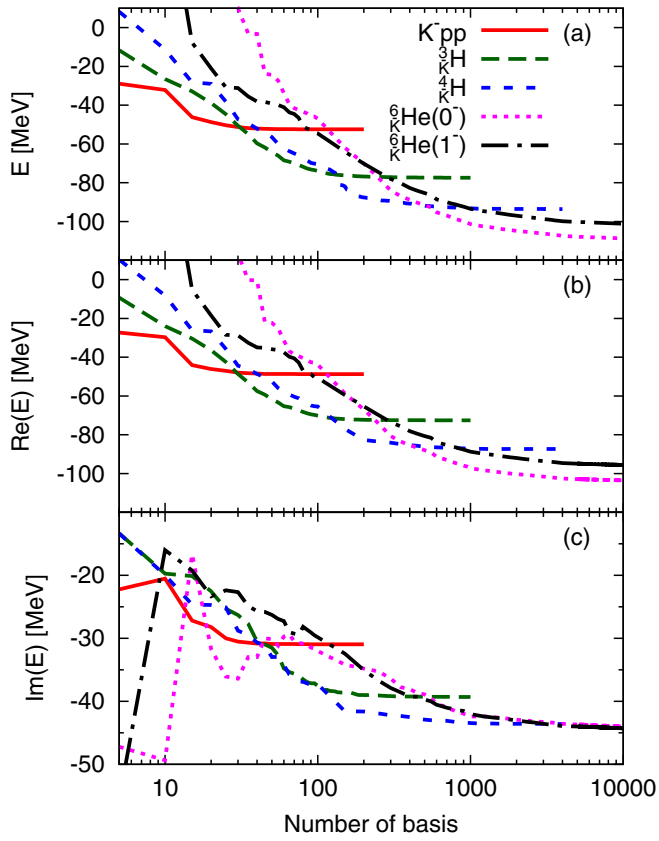

FIG. 1. Energy convergence of the ground states of three- to seven-body systems including an antikaon. (a) Eigenvalues calculated only with the real part of the Hamiltonian; (b) real part of the full Hamiltonian eigenvalue; (c) imaginary part of the full Hamiltonian eigenvalue. The AY potential model is employed as the $\bar{K}N$ interaction. See text for details.

IV. STRUCTURE OF FEW-BODY SYSTEMS

The internal structure of the the $\bar{K}$ nuclei is reflected in the obtained wave function Ψ_{JMM_T}. Here we define several quantities which are useful to investigate the structure of the few-body systems.

We first define the NN root-mean-square (rms) distances $\sqrt{\langle r^2_{NN}\rangle}$, $\bar{K}N$ rms distances $\sqrt{\langle r^2_{\bar{K}N}\rangle}$, N rms radii $\sqrt{\langle r^2_N\rangle}$, and $\bar{K}$ rms radii $\sqrt{\langle r^2_{\bar{K}}\rangle}$ by using the following operators:

$$r^2_{NN} = \sum_{i<j}^{\mathcal{N}-1} \frac{2|\boldsymbol{r}_i - \boldsymbol{r}_j|^2}{(\mathcal{N}-1)(\mathcal{N}-2)}, \tag{26}$$

$$r^2_{\bar{K}N} = \sum_{i}^{\mathcal{N}-1} \frac{|\boldsymbol{r}_{\bar{K}} - \boldsymbol{r}_i|^2}{(\mathcal{N}-1)}, \tag{27}$$

$$r^2_{N} = \sum_{i}^{\mathcal{N}-1} \frac{|\boldsymbol{r}_i - \boldsymbol{x}_{\mathcal{N}}|^2}{(\mathcal{N}-1)}, \tag{28}$$

$$r^2_{\bar{K}} = |\boldsymbol{r}_{\bar{K}} - \boldsymbol{x}_{\mathcal{N}}|^2, \tag{29}$$

where $\boldsymbol{r}_i$ and $\boldsymbol{r}_{\bar{K}} = \boldsymbol{r}_{\mathcal{N}}$ are the single-particle coordinates of the ith nucleon and the antikaon, respectively. The rms distances represent the averaged distance of the two-body subsystems, and the rms radii measure the averaged distance of the particle from the center-of-mass of the total system $\boldsymbol{x}_{\mathcal{N}}$. As discussed in Sec. II, we calculate the expectation values of these operators $\sqrt{\langle r^2\rangle}$ using the standard normalization condition (4).

To investigate how the nuclear system shrinks by adding an antikaon, we define the nucleon density distributions

$$\rho^{N\mathrm{cm}}_N(r) = \sum_{i=1}^{\mathcal{N}-1} \int d\boldsymbol{x} |\Psi_{JMM_T}(\boldsymbol{x})|^2 \delta\big(\boldsymbol{r}^{N\mathrm{cm}}_i - \boldsymbol{r}\big), \tag{30}$$

$$\boldsymbol{r}^{N\mathrm{cm}}_i = \boldsymbol{r}_i - (\boldsymbol{x}_{\mathcal{N}-1} + \boldsymbol{r}_{\bar{K}}), \tag{31}$$

where $\boldsymbol{r}^{N\mathrm{cm}}_i$ denotes the ith nucleon coordinate measured from the center-of-mass system of nucleons; $\rho^{N\mathrm{cm}}_N(r)$ is normalized as $\int 4\pi r^2 \rho^{N\mathrm{cm}}_N(r) = \mathcal{N}-1$. Here, again, we adopt the standard normalization condition (4). The comparison of $\rho^{N\mathrm{cm}}_N(r)$ with the corresponding quantity of the normal nuclei with $\mathcal{N}-1$ nucleons shows the effect of the modification of the distribution of the nucleons by the presence of the antikaon.

We also calculate the nucleon and antikaon density distribution ρ_N and $\rho_{\bar{K}}$ measured from the total center-of-mass system, defined as

$$\rho_N(r) = \sum_{i=1}^{\mathcal{N}-1} \int d\boldsymbol{x} |\Psi_{JMM_T}(\boldsymbol{x})|^2 \delta\big(\boldsymbol{r}^{\mathrm{cm}}_i - \boldsymbol{r}\big), \tag{32}$$

$$\rho_{\bar{K}}(r) = \int d\boldsymbol{x} |\Psi_{JMM_T}(\boldsymbol{x})|^2 \delta\big(\boldsymbol{r}^{\mathrm{cm}}_{\bar{K}} - \boldsymbol{r}\big), \tag{33}$$

where $\boldsymbol{r}^{\mathrm{cm}}_{i(\bar{K})} = \boldsymbol{r}_{i(\bar{K})} - \boldsymbol{x}_{\mathcal{N}}$ is ith nucleon (antikaon) coordinate from the total center-of-mass coordinate $\boldsymbol{x}_{\mathcal{N}}$.

It is also instructive to estimate the fractions of different components in the wave functions. We define the projections onto the component with K^- [Eq. (25)] and that with $\bar{K}^0$ [Eq. (24)] as

$$\hat{P}_{K^-} = \frac{1}{2}\big(1 - \tau^{(3)}_{\mathcal{N}}\big), \tag{34}$$

$$\hat{P}_{\bar{K}^0} = \frac{1}{2}\big(1 + \tau^{(3)}_{\mathcal{N}}\big), \tag{35}$$

with $\hat{P}_{K^-} + \hat{P}_{\bar{K}^0} = 1$. By taking the expectation value of Eq. (4), we obtain the probability of finding each component in the wave function:

$$P_{K^-} = \langle \hat{P}_{K^-}\rangle, \tag{36}$$

$$P_{\bar{K}^0} = \langle \hat{P}_{\bar{K}^0}\rangle. \tag{37}$$

The projection operators can also be used to decompose the eigenenergy into different contributions from each term of the Hamiltonian. For this purpose, we use the Gamow state normalization (7). The expectation values of the kinetic energy and potential energy of the diagonal K^- channel, $\langle T\rangle^{K^-}_G$ and $\langle V\rangle^{K^-}_G$, of the diagonal $\bar{K}^0$ channel, $\langle T\rangle^{\bar{K}^0}_G$ and $\langle V\rangle^{\bar{K}^0}_G$, and of

the off-diagonal K^--$\bar{K}^0$ channel $\langle V\rangle_G^{K^-\bar{K}^0}$ are given by

$$\begin{pmatrix} \langle T+V\rangle_G^{K^-} & \langle V\rangle_G^{K^-\bar{K}^0} \\ \langle V\rangle_G^{K^-\bar{K}^0} & \langle T+V\rangle_G^{\bar{K}^0} \end{pmatrix} \equiv \begin{pmatrix} \langle \hat{P}_{K^-}(T+V)\hat{P}_{K^-}\rangle_G & \langle \hat{P}_{K^-}V\hat{P}_{\bar{K}^0}\rangle_G \\ \langle \hat{P}_{\bar{K}^0}V\hat{P}_{K^-}\rangle_G & \langle \hat{P}_{\bar{K}^0}(T+V)\hat{P}_{\bar{K}^0}\rangle_G \end{pmatrix}. \quad (38)$$

With these definitions, the eigenenergy is decomposed as

$$-B-i\frac{\Gamma}{2} = \langle T\rangle_G^{K^-} + \langle T\rangle_G^{\bar{K}^0} + \langle V\rangle_G^{K^-} + \langle V\rangle_G^{\bar{K}^0} + 2\langle V\rangle_G^{K^-\bar{K}^0}. \quad (39)$$

We also investigate the probability of finding each $\bar{K}N$ isospin component in the wave function by using the following expectation values:

$$P_{\bar{K}N}^{I=0} = \sum_i^{\mathcal{N}-1} \frac{\langle \hat{P}_{i\mathcal{N}}^{I=0}\rangle}{\mathcal{N}-1}, \quad (40)$$

$$P_{\bar{K}N}^{I=1} = \sum_i^{\mathcal{N}-1} \frac{\langle \hat{P}_{i\mathcal{N}}^{I=1}\rangle}{\mathcal{N}-1}. \quad (41)$$

V. RESULTS AND DISCUSSION

A. Structure of strange dibaryon resonances $\bar{K}NN$

We proceed now to investigate the structure of the kaonic nuclei. For the three-body systems, we investigate the structure of the $I = 1/2$ quasibound states for the strange dibaryon resonances $\bar{K}NN$, K^-pp-$\bar{K}^0pn$ and K^-pn-$\bar{K}^0nn$ systems, with $J^\pi = 0^-$ and 1^- in the charge-basis representation. As in the previous studies [22–32], we find one quasibound state below the $\Lambda(1405) + N$ threshold for $J^\pi = 0^-$, but we could not find any states below the threshold for $J^\pi = 1^-$. We summarize the detailed properties of the K^-pp-$\bar{K}^0pn$ and K^-pn-$\bar{K}^0nn$ systems with $J^\pi = 0^-$ in Tables II and III, respectively.

We first compare the results with different choices of the two-body energy (Types I and II) discussed in Sec. II C. The real part of $\delta\sqrt{s}$ with Type II is about a half of that of Type I. The binding energy of K^-pp-$\bar{K}^0pn$ system is not sensitive to the choice of the two-body energy and the values are around 27 MeV. Meanwhile, the decay width of Type I (∼31 MeV) becomes about half of that of Type II (∼59 MeV). The rms distances $\sqrt{\langle r_{NN}^2\rangle}$, $\sqrt{\langle r_{\bar{K}N}^2\rangle}$, $\sqrt{\langle r_N^2\rangle}$, and $\sqrt{\langle r_{\bar{K}}^2\rangle}$ of Type II are slightly smaller than those of Type I. The probabilities of finding several components, P_{K^-}, $P_{\bar{K}^0}$, $P_{\bar{K}N}^{I=0}$, and $P_{\bar{K}N}^{I=1}$ are not sensitive to the choice of the two-body energy.

We obtain the binding energies at 20–30 MeV, which are consistent with recent experimental measurement of the ^{3}He$(K^-,\Lambda p)n$ reaction by J-PARC E15 [47] and its theoretical analysis [48]. The obtained binding energies with the Kyoto $\bar{K}N$ potential are 5–10 MeV larger than the values obtained in Refs. [22,23,25] with the chiral potential constructed in Ref. [18]. This difference mainly comes from the different treatment of the imaginary part of the potential as well as

TABLE II. Properties of the K^-pp-$\bar{K}^0pn$ system with $J^\pi = 0^-$. See text for details.

Model	Kyoto		AY
	Type I	Type II	
B (MeV)	27.9	26.1	48.7
Γ (MeV)	30.9	59.3	61.9
$\delta\sqrt{s}$ (MeV)	$-61.0-i25.0$	$-30.2-i23.7$	
P_{K^-}	0.65	0.65	0.64
$P_{\bar{K}^0}$	0.35	0.35	0.36
$\sqrt{\langle r_{NN}^2\rangle}$ (fm)	2.16	2.07	1.84
$\sqrt{\langle r_{\bar{K}N}^2\rangle}$ (fm)	1.80	1.73	1.55
$\sqrt{\langle r_N^2\rangle}$ (fm)	1.12	1.08	0.958
$\sqrt{\langle r_{\bar{K}}^2\rangle}$ (fm)	1.14	1.10	0.988
$\langle T\rangle_G^{K^-}$ (MeV)	$117+i28.8$	$124+i53.1$	$102+i31.4$
$\langle V\rangle_G^{K^-}$ (MeV)	$-113-i33.7$	$-120-i63.9$	$-102-i47.0$
$\langle T\rangle_G^{\bar{K}^0}$ (MeV)	$74.3+i18.4$	$76.3+i33.1$	$63.1+i15.5$
$\langle V\rangle_G^{\bar{K}^0}$ (MeV)	$-62.0-i19.1$	$-64.3-i35.6$	$-48.6-i21.6$
$2\langle V\rangle_G^{K^-\bar{K}^0}$ (MeV)	$-44.1-i9.76$	$-41.9-i16.4$	$-64.0-i9.24$
$P_{\bar{K}N}^{I=0}$	0.72	0.73	0.73
$P_{\bar{K}N}^{I=1}$	0.28	0.27	0.27

TABLE III. Properties of the K^-pn-$\bar{K}^0nn$ system with $J^\pi = 0^-$.

Model	Kyoto		AY
	Type I	Type II	
B (MeV)	27.6	25.3	48.1
Γ (MeV)	31.6	59.4	61.6
$\delta\sqrt{s}$ (MeV)	$-60.2-i25.6$	$-29.4-i23.8$	
P_{K^-}	0.38	0.38	0.37
$P_{\bar{K}^0}$	0.62	0.62	0.63
$\sqrt{\langle r_{NN}^2\rangle}$ (fm)	2.18	2.10	1.85
$\sqrt{\langle r_{\bar{K}N}^2\rangle}$ (fm)	1.82	1.75	1.56
$\sqrt{\langle r_N^2\rangle}$ (fm)	1.13	1.09	0.963
$\sqrt{\langle r_{\bar{K}}^2\rangle}$ (fm)	1.15	1.11	0.993
$\langle T\rangle_G^{K^-}$ (MeV)	$67.6+i20.6$	$81.4+i34.9$	$65.3+i16.1$
$\langle V\rangle_G^{K^-}$ (MeV)	$-44.5-i10.2$	$-69.9-i38.0$	$-51.3-i22.6$
$\langle T\rangle_G^{\bar{K}^0}$ (MeV)	$112+i28.7$	$118+i52.2$	$99.5+i30.8$
$\langle V\rangle_G^{\bar{K}^0}$ (MeV)	$-107-i33.3$	$-112-i62.2$	$-97.3-i45.8$
$2\langle V\rangle_G^{K^-\bar{K}^0}$ (MeV)	$-44.5-i10.2$	$-42.2-i16.7$	$-64.3-i9.40$
$P_{\bar{K}N}^{I=0}$	0.72	0.72	0.73
$P_{\bar{K}N}^{I=1}$	0.28	0.28	0.27

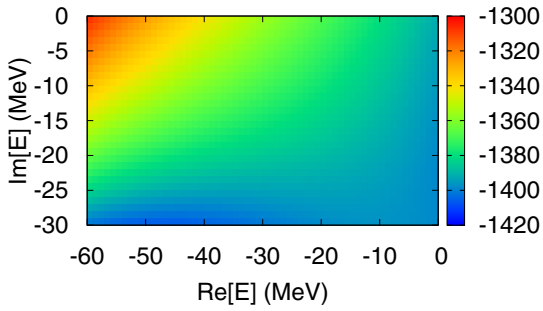

FIG. 2. Real part of the Kyoto $\bar{K}N$ potential, Re $V_{\bar{K}N}^{I=0}(r=0,E)$, on the complex energy plane.

the difference of the potential model. In Refs. [22,23,25], the Schrödinger equation is solved only with the real part of Hamiltonian and the decay width is estimated by taking the expectation value with the imaginary part of the potential, while we solve the Schrödinger equation by direct diagonalization with the full complex Hamiltonian. If we do not take into account the energy dependence of the $\bar{K}N$ potential, the binding energies obtained by direct diagonalization of the complex potential $V_{\bar{K}N}(r,E)$ become smaller than those obtained by using the real part of the potential Re$[V_{\bar{K}N}(r,E)]$. However, the $\bar{K}N$ two-body energy E in the three-body system also becomes a complex value with the complex potential $V_{\bar{K}N}(r,E)$. Considering the energy dependence of the potential, the $\bar{K}N$ interaction $V_{\bar{K}N}(r,E)$ becomes more attractive than the $\bar{K}N$ interaction $V_{\bar{K}N}(r,\mathrm{Re}[E])$ on the real energy axis. This is found in Fig. 2, which plots the real part of $V_{\bar{K}N}$ on the complex energy plane. As a result of self-consistent calculation, the binding energies of the complex potential $V_{\bar{K}N}(r,E)$ become larger than those of only the real part of potential Re$[V_{\bar{K}N}(r,E)]$. Therefore, we obtain binding energies 5–10 MeV larger than those obtained in Refs. [22,23,25].

We then investigate the origin of the binding using the decomposition in Eq. (39). From Tables II and III, we see that $\mathrm{Re}\langle T\rangle_G^{K^-,\bar{K}^0}$ almost cancels out $\mathrm{Re}\langle V\rangle_G^{K^-,\bar{K}^0}$ in both K^- and $\bar{K}^0$ channels. Therefore the K^--$\bar{K}^0$ channel coupling is essential for the energy gain. Meanwhile, both of the diagonal and the off-diagonal components contribute to the decay width.

It is also instructive to decompose the wave function into the isospin components. The dominant isospin component of the $\bar{K}NN$ ground state is considered to have $I_{NN}=1$ and total isospin $I=1/2$. This is because the $I_{\bar{K}N}=0$ channel has stronger attraction than that of the $I_{\bar{K}N}=1$ channel, and the $I_{NN}=1$ channel gives more $I_{\bar{K}N}=0$ component than that of the $I_{NN}=0$ channel [6]. This can easily be explained by recoupling the isospins in the following way:

$$\begin{aligned}&\big[\big[\eta(N)_{\frac{1}{2}}\eta(N)_{\frac{1}{2}}\big]_1\eta(\bar{K})_{\frac{1}{2}}\big]_{\frac{1}{2}}\\&=\frac{\sqrt{3}}{2}\big[\eta(N)_{\frac{1}{2}}\big[\eta(N)_{\frac{1}{2}}\eta(\bar{K})_{\frac{1}{2}}\big]_0\big]_{\frac{1}{2}}\\&+\frac{1}{2}\big[\eta(N)_{\frac{1}{2}}\big[\eta(N)_{\frac{1}{2}}\eta(\bar{K})_{\frac{1}{2}}\big]_1\big]_{\frac{1}{2}},\end{aligned}\tag{42}$$

$$\begin{aligned}&\big[\big[\eta(N)_{\frac{1}{2}}\eta(N)_{\frac{1}{2}}\big]_0\eta(\bar{K})_{\frac{1}{2}}\big]_{\frac{1}{2}}\\&=-\frac{1}{2}\big[\eta(N)_{\frac{1}{2}}v\big[\eta(N)_{\frac{1}{2}}\eta(\bar{K})_{\frac{1}{2}}\big]_0\big]_{\frac{1}{2}}\\&+\frac{\sqrt{3}}{2}\big[\eta(N)_{\frac{1}{2}}\big[\eta(N)_{\frac{1}{2}}\eta(\bar{K})_{\frac{1}{2}}\big]_1\big]_{\frac{1}{2}}.\end{aligned}\tag{43}$$

If the ground state is a pure $I=1$ NN state, the ratio of the probabilities of finding the $\bar{K}N$ $I=0$ and $I=1$ channels is given by $P_{\bar{K}N}^{I=0}:P_{\bar{K}N}^{I=1}=3:1$. We can further decompose this state by the third component of the isospin of the antikaon as

$$\begin{aligned}&\big[\big[\eta(N)_{\frac{1}{2}}\eta(N)_{\frac{1}{2}}\big]_1\eta(\bar{K})_{\frac{1}{2}}\big]_{\frac{1}{2},\frac{1}{2}}\\&=-\sqrt{\frac{2}{3}}\big[\eta(N)_{\frac{1}{2}}\eta(N)_{\frac{1}{2}}\big]_{1,1}\eta(\bar{K})_{\frac{1}{2},-\frac{1}{2}}\\&+\sqrt{\frac{1}{3}}\big[\eta(N)_{\frac{1}{2}}\eta(N)_{\frac{1}{2}}\big]_{1,0}\eta(\bar{K})_{\frac{1}{2},\frac{1}{2}}.\end{aligned}\tag{44}$$

where the first (second) term corresponds to K^-pp ($\bar{K}^0pn$). This leads to the ratio of the probabilities of the K^-pp and

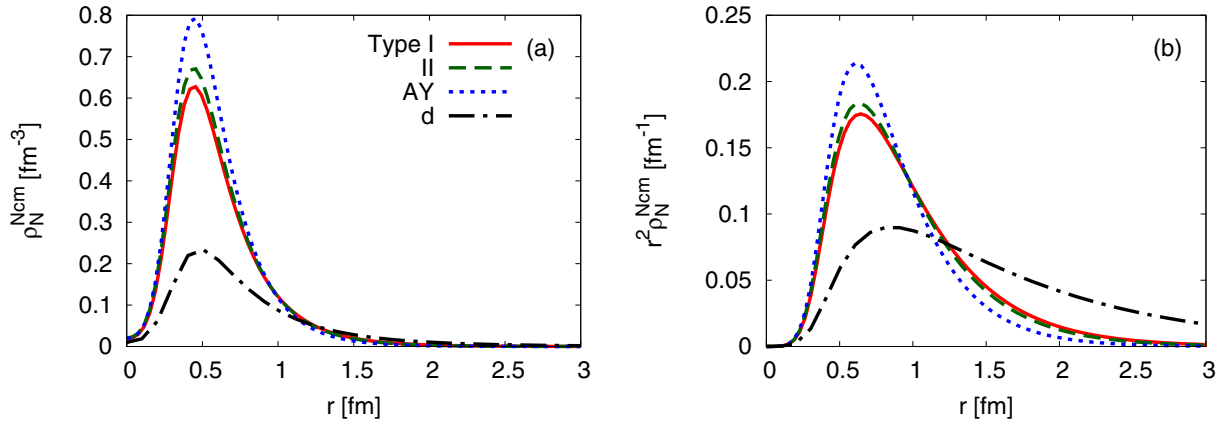

FIG. 3. Nucleon density distributions (a) $\rho_N^{N\mathrm{cm}}(r)$ and (b) $r^2\rho_N^{N\mathrm{cm}}(r)$ for the K^-pp-$\bar{K}^0pn$ system measured from the center-of-mass of nucleons. We employ the Kyoto $\bar{K}N$ potential with the Type-I and -II $\bar{K}N$ two-body energies and the AY potential. The dotted-dashed curves show that of deuteron for comparison. Note that the spin-parity is $J^\pi=0^-$ for $\bar{K}NN$ but $J^\pi=1^+$ for deuteron.

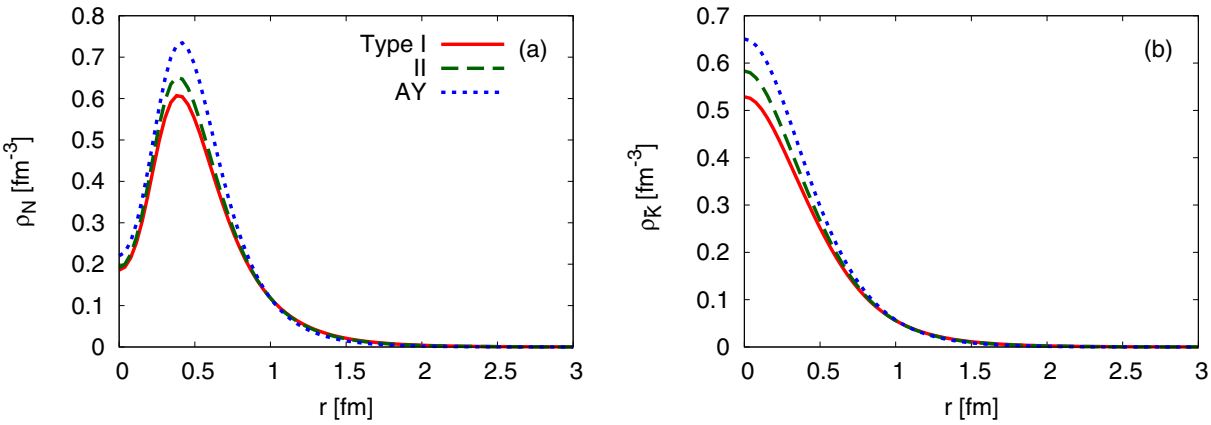

FIG. 4. (a) Nucleon density distribution $\rho_N(r)$ and (b) antikaon density distribution $\rho_{\bar{K}}(r)$ for the $K^- pp$-$\bar{K}^0 pn$ system measured from the center-of-mass of the system. The Kyoto $\bar{K}N$ and AY potentials are employed.

$\bar{K}^0 pn$ components being $P_{K^-} : P_{\bar{K}^0} = 2 : 1$. The obtained $P^I_{\bar{K}N}$'s and $P_{K^-,\bar{K}^0}$ in Tables II and III well satisfy these relations. The small deviations from the ideal ratios 3 : 1 and 2 : 1 come from the contributions of the isospin-singlet NN component with odd wave and the Coulomb interaction that induces the isospin mixing.

Because the Coulomb interaction is included in our formalism, the energy splitting of the two members of the isospin doublet, $K^- pp$-$\bar{K}^0 pn$ and $K^- pn$-$\bar{K}^0 nn$, appears. The splitting between these two systems is very small, $\Delta B = B(K^- pp\text{-}\bar{K}^0 pn) - B(K^- pn\text{-}\bar{K}^0 nn) \sim 0.5$ MeV. There are two attractive and one repulsive Coulombic pairs in the $K^- pp$ channel, and one attractive Coulombic pair in the $K^- pn$ channel. Because $P_{K^-} = 0.65$ in $K^- pp$-$\bar{K}^0 pn$ is much larger than $P_{K^-} = 0.38$ in $K^- pn$-$\bar{K}^0 nn$, the Coulomb interaction affects more attractively the $K^- pp$-$\bar{K}^0 pn$ system than the $K^- pn$-$\bar{K}^0 nn$ system.

Next, we show the particle density distributions of the $K^- pp$-$\bar{K}^0 pn$ system. Figure 3 plots the density distributions of nucleons $\rho_N^{N\mathrm{cm}}(r)$ defined in Eq. (30). The density distribution of the deuteron is also plotted for comparison. The central nucleon density ($r \lesssim 0.3$ fm) is suppressed due to the repulsive core of the nuclear force employed. The nuclear system in the $\bar{K}NN$ system becomes more compact than in the deuteron. The shrinkage effect of nucleons with Type II is slightly stronger than that with Type I. This is because the $\bar{K}N$ interactions with Type II is more attractive than those with Type I due to different $\delta\sqrt{s}$. In Fig. 4, we also show the nucleon and antikaon density distributions ρ_N and $\rho_{\bar{K}}$ defined in Eqs. (32) and (33). The nucleon density is suppressed around the origin, while the antikaon density distribution is not suppressed since there is no repulsive core in the $\bar{K}N$ potential.

We also perform the same calculations by employing the phenomenological potential model: the Akaishi-Yamazaki (AY) potential [4,27]. The results are shown in Tables II and III and Figs. 3 and 4. The AY potential is more attractive than the Kyoto $\bar{K}N$ potential in the subthreshold energy region. The binding energies of the $\bar{K}NN$ systems are approximately twice those with the Kyoto $\bar{K}N$ potential, and the decay widths are $\Gamma \sim 62$ MeV. The particle density distributions become more compact, and the rms radii are about 0.85 times smaller than those for the Kyoto $\bar{K}N$ potential. Our results for AY potential are comparable with the results in Ref. [27].

B. Structure of $\bar{K}NNN$ quasibound state

Next, we investigate the structure of the four-body system, the strange tribaryon $\bar{K}NNN$ system with $J^\pi = 1/2^-$. We find a quasibound state in the $K^- ppn$-$\bar{K}^0 pnn$ coupled system ($\equiv {}^3_{\bar{K}}\mathrm{H}$). Our results are listed in Table IV. We also investigate the $K^- ppp$-$\bar{K}^0 ppn$ coupled system ($\equiv {}^3_{\bar{K}}\mathrm{He}$) with $J^\pi = 1/2^-$, but we do not find any states below the $(\bar{K}NN) + N$ threshold.

TABLE IV. Properties of the ${}^3_{\bar{K}}\mathrm{H}$ system with $J^\pi = 1/2^-$.

Model	Kyoto		AY
	Type I	Type II	
B (MeV)	45.3	49.7	72.6
Γ (MeV)	25.5	69.4	78.6
$\delta\sqrt{s}$ (MeV)	$-70.4 - i20.7$	$-26.1 - i18.6$	
P_{K^-}	0.53	0.53	0.51
$P_{\bar{K}^0}$	0.47	0.47	0.49
$\sqrt{\langle r^2_{NN}\rangle}$ (fm)	1.99	1.90	1.87
$\sqrt{\langle r^2_{\bar{K}N}\rangle}$ (fm)	1.79	1.68	1.63
$\sqrt{\langle r^2_{N}\rangle}$ (fm)	1.17	1.11	1.09
$\sqrt{\langle r^2_{\bar{K}}\rangle}$ (fm)	1.17	1.08	1.03
$\langle T\rangle^{K^-}_G$ (MeV)	$114 + i17.4$	$126 + i42.2$	$107 + i27.6$
$\langle V\rangle^{K^-}_G$ (MeV)	$-118 - i22.4$	$-135 - i54.0$	$-114 - i44.6$
$\langle T\rangle^{\bar{K}^0}_G$ (MeV)	$103 + i15.9$	$113 + i39.8$	$101 + i26.1$
$\langle V\rangle^{\bar{K}^0}_G$ (MeV)	$-105 - i20.2$	$-118 - i50.0$	$-107 - i42.1$
$2\langle V\rangle^{K^-\bar{K}^0}_G$ (MeV)	$-39.0 - i3.56$	$-36.0 - i12.7$	$-59.6 - i6.33$
$P^{I=0}_{\bar{K}N}$	0.50	0.50	0.50
$P^{I=1}_{\bar{K}N}$	0.50	0.50	0.50

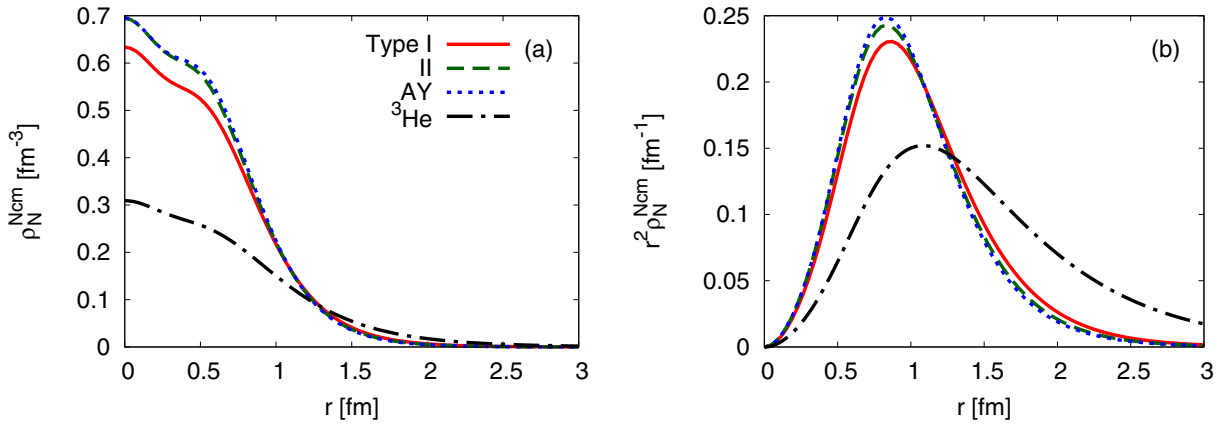

FIG. 5. Same as Fig. 3 but for the ${}^{3}_{\bar{K}}$H system. The nucleon density distributions for ^{3}He is plotted for comparison.

The dependence of the choice of the two-body energy (Types I and II) shows a similar trend with that in the three-body sector. For Type II the real part of $\delta\sqrt{s}$ is less than a half of those with Type I. Therefore the $\bar{K}N$ attraction with Type II is stronger than that with Type I, and the binding energy with Type II is larger than that with Type I. The decay width with Type II ($\sim$69 MeV) becomes around three times as large as that with Type I ($\sim$26 MeV). The obtained binding energies by using the Kyoto $\bar{K}N$ potential are 15$-$20 MeV larger than the values obtained in Ref. [25]. As discussed in the three-body sector, this difference mainly comes from the different treatment of the imaginary part of the potential as well as the difference of the potential model. Since the number of $\bar{K}N$ pairs is larger, the effects of those differences are stronger in the four-body systems than those in the three-body systems.

The rms distances $\sqrt{\langle r_{NN}^2\rangle}$, $\sqrt{\langle r_{\bar{K}N}^2\rangle}$, $\sqrt{\langle r_N^2\rangle}$, and $\sqrt{\langle r_{\bar{K}}^2\rangle}$ with Type II are slightly smaller than those with Type I, in accordance with the larger binding. The probabilities of finding the K^-ppn (P_{K^-}) and $\bar{K}^0pnn$ ($P_{\bar{K}^0}$) channels are not sensitive to the choice of the two-body energies. A large contribution to the real part from $2\langle V\rangle_G^{K^-\bar{K}^0}$ indicates that the K^--$\bar{K}^0$ channel coupling is essential for gaining the binding energy for four-body systems, while the diagonal channels also give contributions to the decay width.

The K^-ppn and $\bar{K}^0pnn$ channels are isospin mirror states. Therefore, the probabilities of these two components follow $P_{K^-} : P_{\bar{K}^0} = 1 : 1$ with the isospin symmetric $\bar{K}N$ and NN interactions. In fact, the numerical results in Table IV are consistent with this expectation within a small isospin mixing by the Coulomb interaction. There are two attractive and one repulsive Coulombic pairs in the K^-ppn channel, while there are no Coulomb interacting pairs in the $\bar{K}^0pnn$ channel. The Coulomb interaction in total affects attractive in the K^-ppn channel, and P_{K^-} becomes slightly larger than $P_{\bar{K}^0}$.

Figure 5 displays $\rho_N^{N\mathrm{cm}}(r)$ and $r^2\rho_N^{N\mathrm{cm}}(r)$ of the ${}^{3}_{\bar{K}}$H system. In the $\bar{K}NNN$ system, the nuclear system becomes more compact, and the central density becomes about two times larger than that in the ^{3}He. Since the $\bar{K}N$ interaction with Type II is more attractive than that with Type I due to small magnitude of the real part of $\delta\sqrt{s}$, the shrinkage effect of nucleons with Type II is slightly stronger than that with Type I. In Fig. 6, we show the nucleon and antikaon density distributions, ρ_N and $\rho_{\bar{K}}$. Those density distributions are similar to each other, and the antikaon rms radius $\sqrt{\langle r_{\bar{K}}^2\rangle}$ is comparable with the nucleon rms radius $\sqrt{\langle r_N^2\rangle}$. The antikaon

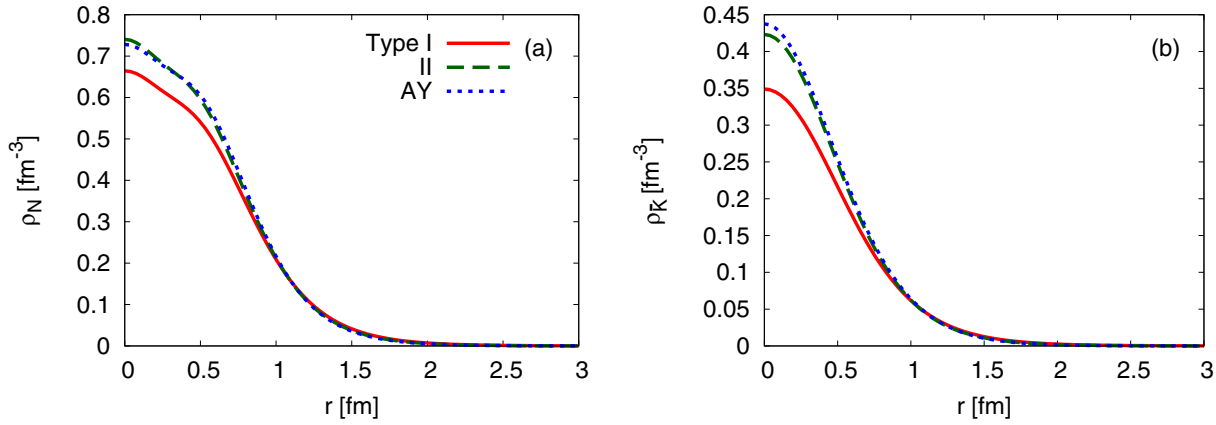

FIG. 6. Same as Fig. 4 but for the ${}^{3}_{\bar{K}}$H system.

moves in the whole region of the nuclear system in order to gain the energy from the strong $\bar{K}N$ interaction.

With the AY potential, the binding energy of the $\bar{K}NNN$ system is about 30 MeV larger than the binding energies with the Kyoto $\bar{K}N$ potential, and the decay width is $\Gamma \sim 79$ MeV. The particle density distributions and the rms radii are similar to those obtained with the Kyoto $\bar{K}N$ potential with Type II, although there is about 30 MeV difference between the binding energies with these two potentials. The tail of the wave function is considered to be related to the binding energy, but the central densities and rms radii are not determined only by the binding energy. It is now clear that the deeply bound ($B >$ 100 MeV in Refs. [6,7]) and high density (8.2 times the normal density shown in Ref. [7]) $\bar{K}NNN$ state is not realized in the accurate few-body calculation. Such an extreme result can be regarded as an artifact due to the approximated treatment of the few-body systems, e.g., the optical potential or the g-matrix approach [6,7] which makes the NN repulsive core soft. A detailed discussion on the effect of the NN repulsive core in the light kaonic nuclei will be given in the following section V D. We, however, emphasize that the existence of the bound state is confirmed also with the realistic Kyoto $\bar{K}N$ interaction, and the central density of nucleons can be about two times larger than that in the ^{3}He.

C. Structure of $\bar{K}NNNN$ quasibound state

Next, we investigate the structure of the five-body systems, strange tetrabaryon $\bar{K}NNNN$ systems with $J^\pi = 0^-$. We find isospin-doublet quasibound states in the $K^- pppn$-$\bar{K}^0 ppnn$ ($\equiv {}^4_{\bar{K}}$He) and $K^- ppnn$-$\bar{K}^0 pnnn$ ($\equiv {}^4_{\bar{K}}$H) systems. Our results are listed in Tables V and VI.

TABLE V. Properties of the ${}^4_{\bar{K}}$He system with $J^\pi = 0^-$.

Model	Kyoto		AY
	Type I	Type II	
B (MeV)	67.9	72.7	85.2
Γ (MeV)	28.3	74.1	86.5
$\delta\sqrt{s}$ (MeV)	$-67.6 - i23.0$	$-18.4 - i15.0$	
P_{K^-}	0.08	0.06	0.16
$P_{\bar{K}^0}$	0.92	0.94	0.84
$\sqrt{\langle r^2_{NN}\rangle}$ (fm)	1.98	1.91	2.07
$\sqrt{\langle r^2_{\bar{K}N}\rangle}$ (fm)	1.83	1.72	1.81
$\sqrt{\langle r^2_{N}\rangle}$ (fm)	1.22	1.18	1.27
$\sqrt{\langle r^2_{\bar{K}}\rangle}$ (fm)	1.22	1.12	1.14
$\langle T\rangle^{K^-}_G$ (MeV)	$32.6 + i6.75$	$26.7 + i16.2$	$50.3 + i7.22$
$\langle V\rangle^{K^-}_G$ (MeV)	$-25.1 - i6.74$	$-20.0 - i15.9$	$-42.3 - i12.0$
$\langle T\rangle^{\bar{K}^0}_G$ (MeV)	$214 + i27.8$	$240 + i66.0$	$183 + i52.7$
$\langle V\rangle^{\bar{K}^0}_G$ (MeV)	$-265 - i38.4$	$-300 - i94.3$	$-232 - i88.3$
$2\langle V\rangle^{K^-\bar{K}^0}_G$ (MeV)	$-24.8 - i3.66$	$-20.2 - i9.13$	$-43.9 - i2.82$
$P^{I=0}_{\bar{K}N}$	0.28	0.27	0.31
$P^{I=1}_{\bar{K}N}$	0.72	0.73	0.69

TABLE VI. Properties of the ${}^4_{\bar{K}}$H system with $J^\pi = 0^-$.

Model	Kyoto		AY
	Type I	Type II	
B (MeV)	69.6	75.5	87.4
Γ (MeV)	28.0	74.5	87.2
$\delta\sqrt{s}$ (MeV)	$-68.7 - i22.4$	$-19.1 - i14.9$	
P_{K^-}	0.93	0.94	0.86
$P_{\bar{K}^0}$	0.07	0.06	0.14
$\sqrt{\langle r^2_{NN}\rangle}$ (fm)	1.96	1.89	2.04
$\sqrt{\langle r^2_{\bar{K}N}\rangle}$ (fm)	1.82	1.71	1.79
$\sqrt{\langle r^2_{N}\rangle}$ (fm)	1.21	1.17	1.26
$\sqrt{\langle r^2_{\bar{K}}\rangle}$ (fm)	1.21	1.11	1.13
$\langle T\rangle^{K^-}_G$ (MeV)	$216 + i28.1$	$244 + i66.6$	$188 + i53.4$
$\langle V\rangle^{K^-}_G$ (MeV)	$-269 - i39.1$	$-306 - i95.7$	$-241 - i90.0$
$\langle T\rangle^{\bar{K}^0}_G$ (MeV)	$30.5 + i5.50$	$25.1 + i14.7$	$47.0 + i6.54$
$\langle V\rangle^{\bar{K}^0}_G$ (MeV)	$-23.0 - i5.54$	$-18.5 - i14.2$	$-38.7 - i10.9$
$2\langle V\rangle^{K^-\bar{K}^0}_G$ (MeV)	$-24.4 - i3.00$	$-19.9 - i8.71$	$-42.7 + i2.64$
$P^{I=0}_{\bar{K}N}$	0.28	0.27	0.30
$P^{I=1}_{\bar{K}N}$	0.72	0.73	0.70

The binding energy with Type II is 5 MeV larger than that with Type I. The decay width with Type II (∼75 MeV) is about three times larger than that with Type I (∼28 MeV). The rms distances $\sqrt{\langle r^2_{NN}\rangle}$, $\sqrt{\langle r^2_{\bar{K}N}\rangle}$, $\sqrt{\langle r^2_{N}\rangle}$, and $\sqrt{\langle r^2_{K}\rangle}$ with Type II are smaller than those with Type I. The probabilities P_{K^-} and $P_{\bar{K}^0}$ are not sensitive to the choice of Types I and II. In contrast to these features, the energy decomposition of the $\bar{K}NNNN$ exhibits different characteristics from the three- and four-body systems. The incomplete cancellation of the kinetic energy and potential energy in the dominant component ($\langle T\rangle^{\bar{K}^0}_G + \langle K\rangle^{\bar{K}^0}_G$ in ${}^4_{\bar{K}}$He and $\langle T\rangle^{K^-}_G + \langle K\rangle^{K^-}_G$ in ${}^4_{\bar{K}}$H) leaves sizable contributions to the binding energy, which are comparable with the off-diagonal components $2\langle V\rangle^{K^-\bar{K}^0}_G$. For the decay widths, the diagonal channels are also important as in the four-body systems.

From the results of P_{K^-} and $P_{\bar{K}^0}$, we see that the dominant component in the ${}^4_{\bar{K}}$He (${}^4_{\bar{K}}$H) system is the $\bar{K}^0 ppnn$ ($K^- ppnn$) channel, although the $K^- pppn$ ($\bar{K}^0 pnnn$) channel contains more $\bar{K}N$ $I = 0$ components than the $\bar{K}^0 ppnn$ ($K^- ppnn$) channel. This is because the nucleon contribution of the $\bar{K}^0 ppnn$ ($K^- ppnn$) channel, which can form an α-particle configuration giving the binding energy about 30 MeV, is larger than the nucleon contribution of the $K^- pppn$ ($\bar{K}^0 pnnn$) channel, and thus the $\bar{K}^0 ppnn$ ($K^- ppnn$) channel is favored. It is also for this reason that the $\bar{K}^0$ (K^-) diagonal component gains the binding energy in the ${}^4_{\bar{K}}$He (${}^4_{\bar{K}}$H) system, as we see above.

The Coulomb splitting between these two systems is larger than that in the $\bar{K}NN$ systems, $\Delta B = B({}^4_{\bar{K}}\text{He}) - B({}^4_{\bar{K}}\text{H}) \sim$ 2 MeV. There is one repulsive Coulombic pair in the $\bar{K}^0 ppnn$

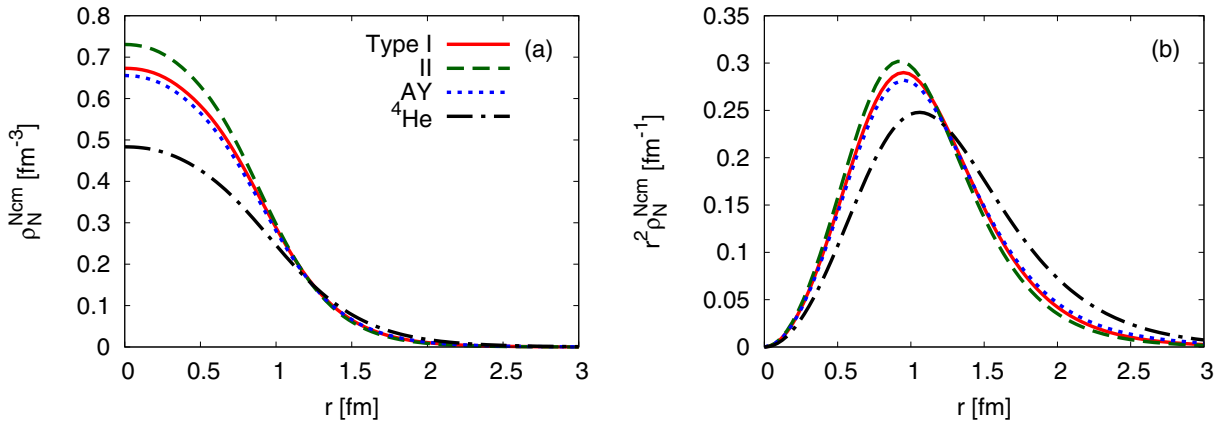

FIG. 7. Same as Fig. 3 but for the ${}^4_{\bar{K}}$H system. The nucleon density distribution for ^{4}He is plotted for comparison.

channel which is the dominant component of the ${}^4_{\bar{K}}$He system, and two attractive and one repulsive Coulombic pairs in the $K^- ppnn$ channel which is the dominant component of the ${}^4_{\bar{K}}$H system. Therefore, Coulomb interaction is repulsive in the ${}^4_{\bar{K}}$He system and attractive in the ${}^4_{\bar{K}}$H system, and the Coulomb splitting becomes larger than that of the three-body systems.

Figures 7 and 8 plot the particle density distributions in the ${}^4_{\bar{K}}$H system. The nucleons in the $\bar{K}NNNN$ system become more compact, and the central density increases to about 1.3–1.5 times higher than that in the ^{4}He. As in the three- and four-body systems, the shrinkage effect of nucleons with Type II is slightly stronger than that with Type I. The antikaon density distribution is similar to the nucleon density distribution.

When we use the AY potential, the binding energies of the $\bar{K}NNNN$ system are about 12–24 MeV larger than those with the Kyoto $\bar{K}N$ potential. Because the quasibound state appears above the $\pi\Sigma NNN$ threshold, it has a sizable decay width of about $\Gamma \sim 87$ MeV, in contrast to the narrow state predicted in Ref. [4]. The probability P_{K^-} ($P_{\bar{K}^0}$) in the ${}^4_{\bar{K}}$He (${}^4_{\bar{K}}$H) system becomes larger than the result with the Kyoto $\bar{K}N$ potential because the AY potential model has more attractive $\bar{K}N$ $I = 0$ interaction than that in the Kyoto $\bar{K}N$ potential. As a result, $P^{I=0}_{\bar{K}N}$ is enhanced. The rms radius of the antikaon is smaller than the corresponding result of the Kyoto $\bar{K}N$ potential with Type I, whereas the nucleon radius is slightly larger.

D. Nuclear force dependence

Here we discuss the NN interaction dependence of our results by comparing the results with the AV4′ potential and those with other NN interaction models such as the Afnan-Tang S3 (ATS3) [49] and Minnesota (MN) potential models [50]. These potential models are often used in studying light nuclei, and well reproduce the binding energy of the s-shell nuclei. It is noted that the strengths of the repulsive core are quite different between these three models as displayed in Fig. 9. The AV4′ potential has the strongest repulsive core, which is comparable to the realistic nuclear forces such as the Argonne V18 potential model [51]. The ATS3 potential model has also a strong short-range repulsion at around the origin. The repulsive core of the MN potential is quite soft. Since the $\bar{K}N$ interaction is strongly attractive, and the kaonic nuclei become more compact than ordinary nuclei. Therefore, there is a possibility that these different repulsive cores affect the results of the kaonic nuclei.

Figure 10 displays the binding energies and decay widths of the $K^- pp$-$\bar{K}^0 pn$ ($J^\pi = 0^-$), ${}^3_{\bar{K}}$H ($J^\pi = 1/2^-$) and ${}^4_{\bar{K}}$H

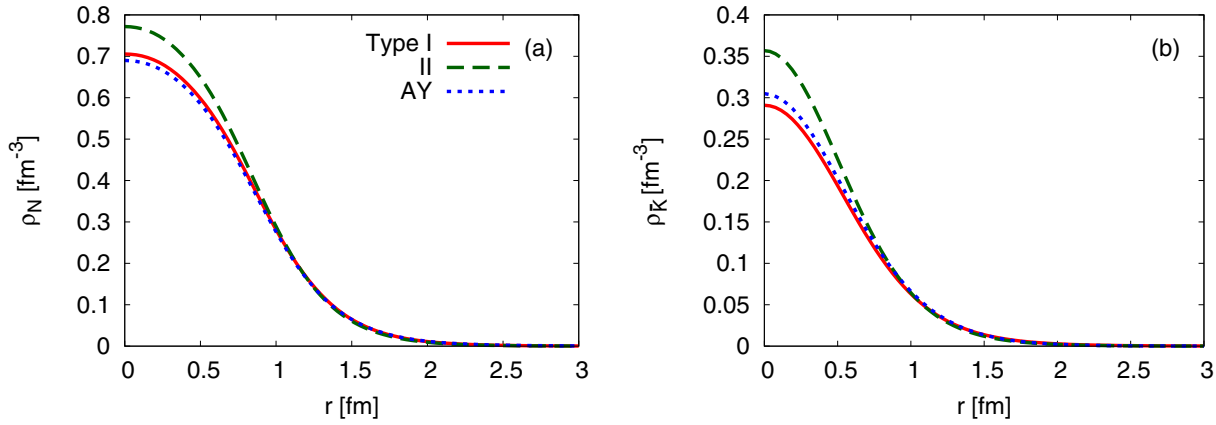

FIG. 8. Same as Fig. 4 but for the ${}^4_{\bar{K}}$H system.

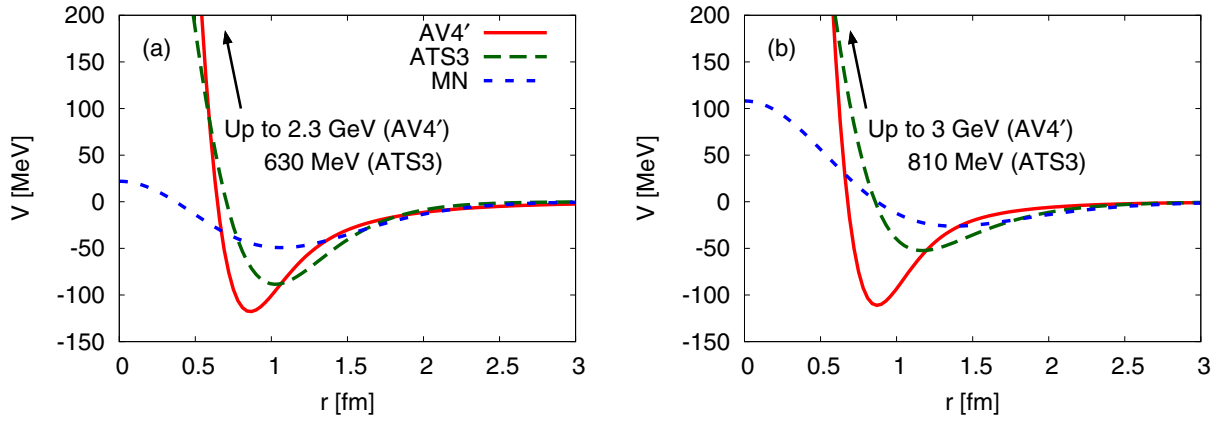

FIG. 9. (a) $^3S_1$ and (b) $^1S_0$ channels of the AV4′, ATS3, and MN NN potentials.

($J^\pi = 0^-$) systems with those three types of nuclear forces. Here, we use the Kyoto $\bar{K}N$ potential as the $\bar{K}N$ potential, and the energy dependence of the potential is determined by Type I. The binding energies and decay widths are almost the same in those with three nuclear forces as well as the binding energies of ordinary s-shell nuclei without the antikaon, as listed in Table VII.

The qualitative difference becomes apparent in the density distributions. Figures 11 and 12 plot the nucleon and antikaon density distributions of the $K^- pp$-$\bar{K}^0 pn$ ($J^\pi = 0^-$), ${}^3_{\bar{K}}$H ($J^\pi = 1/2^-$), and ${}^4_{\bar{K}}$H ($J^\pi = 0^-$) systems. The density distributions with the AV4′ potential model are similar to those with the ATS3 model, while the central densities with the MN potential with repulsive core are significantly higher than those for the other potential models. Since the short-range repulsive core of the MN potential is not as strong as those of the other potential models, nucleons can come very close to each other due to the strong $\bar{K}N$ attraction. In the ${}^3_{\bar{K}}$H system, the central density obtained with the MN potential model becomes $\rho_N^{N\mathrm{cm}}(r=0) \sim 1.2\ \mathrm{fm}^{-3}$, approximately two times larger than those with the AV4′ and ATS3 potential models. The value is close to $1.4\ \mathrm{fm}^{-3}$ predicted in Refs. [7,8] by using the antisymmetrized-molecular-dynamics calculation with the effective treatment of the $\bar{K}N$ and NN interactions with the g matrix. Since the $\bar{K}N$ interaction is very strong, the nucleons can be compressed too much with a soft core potential and form such an unrealistically high density state. Use of a realistic nuclear force is necessary in order to avoid such an artificial solution.

E. $\bar{K}NNNNN$ quasibound state

For the six-body $\bar{K}NNNNN$ systems, we could not find any states below the strange tetrabaryon and a nucleon $(\bar{K}NNNN) + N$ threshold energy in the $L = 0$ state. Since the ^{5}He ground state is observed as a resonant state with $J^\pi = 3/2^-$, the orbital angular momentum of the ground state is expected to be $L = 1$.

Investigation with $L > 0$ states is possible by introducing the global vectors that efficiently describe the rotational motion of the system with any L^π [34,36,52,53], but this extension is beyond the scope of this paper.

F. Structure of $\bar{K}NNNNNN$ quasibound state

Finally, we investigate the structure of the seven-body systems, strange hexabaryon $\bar{K}NNNNNN$. The ground state of the six-nucleon systems without an antikaon is ^{6}Li with $J^\pi = 1^+$, and the $J^\pi = 0^+$ isospin-triplet states, ^{6}He, ^{6}Li and ^{6}Be, are the excited states. By adding an antikaon, we can construct two isospin doublets with $J^\pi = 1^-$ and 0^-. We find quasibound states in these quantum numbers, while we do not find any states below the $(\bar{K}NNNN) + 2N$ threshold for

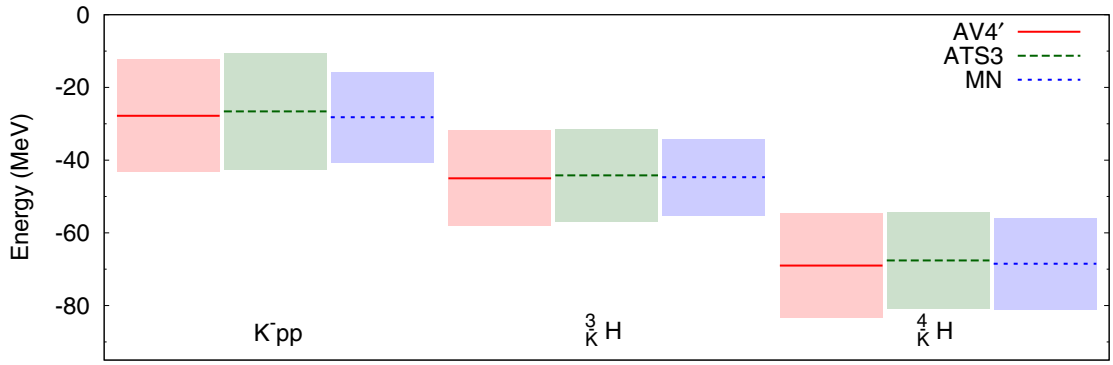

FIG. 10. Energy levels of $K^- pp(J^\pi = 0^-)$, ${}^3_{\bar{K}}\mathrm{H}(J^\pi = 1/2^-)$, and ${}^4_{\bar{K}}\mathrm{H}(J^\pi = 0^-)$ systems with the AV4′, ATS3, and MN potentials. The shaded widths represent the decay widths. The Kyoto $\bar{K}N$ potential with Type I is employed for the $\bar{K}N$ interaction.

TABLE VII. Total binding energies B and decay widths Γ of ordinary nuclei and kaonic nuclei. The Kyoto $\bar{K}N$ potential with Type I is employed for the $\bar{K}N$ interaction.

	B (MeV)				(B,Γ) (MeV)		
	AV4′	ATS3	MN		AV4′	ATS3	MN
^{2}H	2.24	2.22	2.20	K^-pp-$\bar{K}^0pn$	(27.9,30.9)	(26.6,32.0)	(28.4,23.9)
^{3}He	8.33	8.11	7.72	${}^{3}_{\bar{K}}$H	(45.3,25.5)	(44.6,25.0)	(45.7,19.3)
^{4}He	32.1	30.8	30.0	${}^{4}_{\bar{K}}$H	(69.6,28.0)	(68.7,26.0)	(68.6,24.6)

$I = 3/2$ with $J^\pi = 0^-$, such as the $K^-ppnnnn$-$\bar{K}^0pnnnnn$ ($\equiv {}^{6}_{\bar{K}}$H) system.

Tables VIII, IX, X, and XI list our results of the $K^-pppppn$-$\bar{K}^0pppnnn$ ($\equiv {}^{6}_{\bar{K}}$Li) system with $J^\pi = 0^-$, the $K^-pppnnn$-$\bar{K}^0ppnnnn$ ($\equiv {}^{6}_{\bar{K}}$He) system with $J^\pi = 0^-$, the ${}^{6}_{\bar{K}}$Li system with $J^\pi = 1^-$, and the ${}^{6}_{\bar{K}}$He system with $J^\pi = 1^-$, respectively. The binding energies for the $J^\pi = 0^-$ (1^-) states with Type II are 9–10 MeV (7–8 MeV) larger than those with Type I. The decay widths with Type II are three times larger than those with Type I. The rms distances $\sqrt{\langle r^2_{NN}\rangle}$, $\sqrt{\langle r^2_{\bar{K}N}\rangle}$, $\sqrt{\langle r^2_{N}\rangle}$, and $\sqrt{\langle r^2_{\bar{K}}\rangle}$ with Type II are slightly smaller than those with Type I. The probabilities P_{K^-} and $P_{\bar{K}^0}$ are not sensitive to the choice of Types I and II. As in the case of four- and five-body systems, the diagonal channels give important contributions to the decay width. In contrast, both of the diagonal and the off-diagonal components produce about a half of the binding energy. The diagonal components of the channel with ^{6}Li, that is, the K^- channel in ${}^{6}_{\bar{K}}$He and the $\bar{K}^0$ channel in ${}^{6}_{\bar{K}}$Li, are important especially for the $J^\pi = 1^-$ states.

The dominant component of the ${}^{6}_{\bar{K}}$Li (${}^{6}_{\bar{K}}$He) system with $J^\pi = 0^-$ is the $K^-pppppn$ ($\bar{K}^0ppnnnn$) channel, while that of the ${}^{6}_{\bar{K}}$Li (${}^{6}_{\bar{K}}$He) system with $J^\pi = 1^-$ is the $\bar{K}^0pppnnn$ ($K^-pppnnn$) channel. For the spin-singlet states ($J^\pi = 0^-$), the core nuclei in ${}^{6}_{\bar{K}}$Li and ${}^{6}_{\bar{K}}$He are the isospin-triplet states of ^{6}Be, ^{6}Li, and ^{6}He, and the channels with larger fraction of the $\bar{K}N$ $I = 0$ components are favored. Meanwhile, for the spin-triplet states ($J^\pi = 1^-$), the core nucleus with $J^\pi = 1^+$ ($\sim{}^6$Li) is the isospin-singlet state. The spin-triplet ^{6}Li is the ground state of the six-nucleon systems, while ^{6}Be and ^{6}He with $J^\pi = 1^+$ are not bound. Therefore, the nucleons in the $\bar{K}^0pppnnn$ ($K^-pppnnn$) channel feel larger attraction than that in the other channel. This determines the dominant component in the $J^\pi = 1^-$ state. This is also the reason why the $\bar{K}^0$ (K^-) diagonal component gains the large binding energy in the spin-singlet ${}^{6}_{\bar{K}}$Li (${}^{6}_{\bar{K}}$He) system, similar to the $\bar{K}NNNN$ system.

The Coulomb splitting between ${}^{6}_{\bar{K}}$Li and ${}^{6}_{\bar{K}}$He in the $J^\pi = 0^-$ channel (0.3–0.8 MeV) is smaller than the splitting in $J^\pi = 1^-$ (2.0–3.2 MeV). In the dominant $K^-pppppn$ component of ${}^{6}_{\bar{K}}$Li with $J^\pi = 0^-$, there are four attractive and six repulsive Coulombic pairs, while the dominant $\bar{K}^0ppnnnn$ channel in ${}^{6}_{\bar{K}}$He contains one repulsive pair. Therefore, the Coulomb interaction in ${}^{6}_{\bar{K}}$Li system is expected to be slightly more repulsive than the ${}^{6}_{\bar{K}}$He system. On the other hand, in the dominant $\bar{K}^0pppnnn$ component of the ${}^{6}_{\bar{K}}$Li system with $J^\pi = 1^-$, there are three repulsive Coulombic pairs, and the dominant $K^-pppnnn$ channel in ${}^{6}_{\bar{K}}$He has three attractive and three repulsive pairs. In the ${}^{6}_{\bar{K}}$He system, the rms distance $\sqrt{\langle r^2_{\bar{K}N}\rangle}$ is smaller than $\sqrt{\langle r^2_{NN}\rangle}$, and therefore the $\bar{K}N$ Coulomb attraction is stronger than the NN repulsion, and the Coulomb interaction works in total attractively in the $K^-pppnnn$ channel. Therefore, the Coulomb splitting between ${}^{6}_{\bar{K}}$Li and ${}^{6}_{\bar{K}}$He in $J^\pi = 1^-$ becomes larger than the splitting in $J^\pi = 0^-$.

Next, we compare the spin-singlet and triplet states. With Type I, the binding energy of ${}^{6}_{\bar{K}}$Li with $J^\pi = 1^-$ is 1 MeV larger than the $J^\pi = 0^-$ state, and ${}^{6}_{\bar{K}}$He with $J^\pi = 1^-$ is 2.2 MeV larger than in $J^\pi = 0^-$. With Type II, the binding energy of ${}^{6}_{\bar{K}}$Li with $J^\pi = 1^-$ is 2.2 MeV smaller than the $J^\pi = 0^-$ state, and ${}^{6}_{\bar{K}}$He with $J^\pi = 1^-$ is 0.8 MeV larger than the $J^\pi = 0^-$ state. Except for ${}^{6}_{\bar{K}}$Li with Type II, the binding energies of the spin-triplet states are larger than the spin-singlet states. This is in accordance with the level structure of the

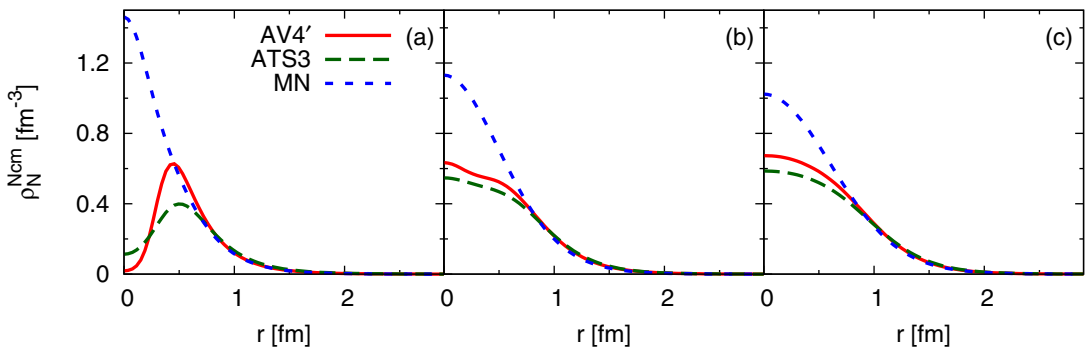

FIG. 11. Nucleon density distribution measured from the center-of-mass system of nucleons for (a) K^-pp, (b) ${}^{3}_{\bar{K}}$H, and (c) ${}^{4}_{\bar{K}}$H systems with the AV4′, ATS3, and MN potentials. The Kyoto $\bar{K}N$ potential with Type I is employed for the $\bar{K}N$ interaction.

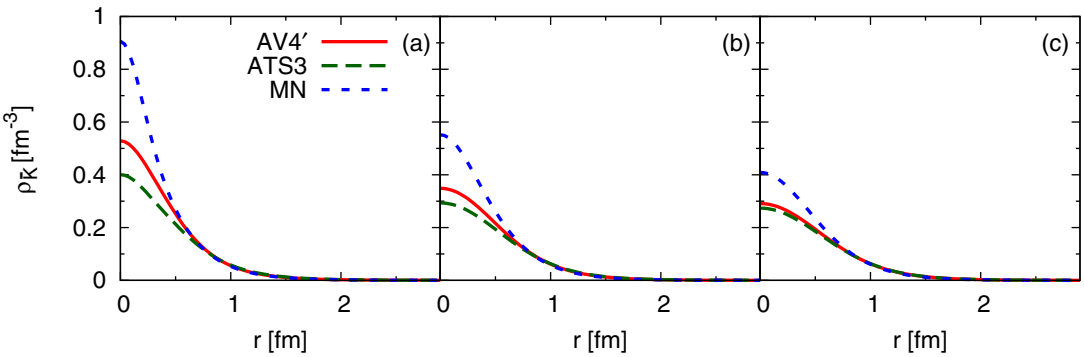

FIG. 12. Antikaon density distribution $\rho_{\bar{K}}(r)$ in the center-of-mass system for (a) $K^- pp$, (b) ${}^{3}_{\bar{K}}\mathrm{H}$, and (c) ${}^{4}_{\bar{K}}\mathrm{H}$ systems. The Kyoto $\bar{K}N$ potential with Type I is employed for the $\bar{K}N$ interaction.

six-nucleon systems. With Type II, the magnitude of the real part of $\delta\sqrt{s}$ used in the two-body $\bar{K}N$ interaction is smaller, and the $\bar{K}N$ interaction becomes more attractive than that with Type I. Because the $J^\pi = 0^-$ state contains a larger fraction of the $I = 0$ $\bar{K}N$ components than the $J^\pi = 1^-$ state, as in the case of the strange dibaryon $\bar{K}NN$ systems, the $\bar{K}N$ interaction with Type II is so strong that the binding energy of ${}^{6}_{\bar{K}}\mathrm{Li}$ with $J^\pi = 0^-$ becomes larger than the $J^\pi = 1^-$ state. In other words, by adding an antikaon, the spin of the ground state of the six-nucleon system may change depending on the strength of the $\bar{K}N$ interaction. The inversion of the level structure of the ground state and the first excited state by the antikaon is also seen in the two-nucleon systems (strange dibaryon $\bar{K}NN$). The ground state of the two-nucleon sector without the antikaon is the spin-triplet deuteron, while the spin-singlet channel is unbound. As discussed in Sec. V A, by injecting an antikaon, the ground state is spin singlet which maximizes the fraction of the $\bar{K}N(I = 0)$ component. Recalling that the ${}^{6}\mathrm{He}$ and ${}^{6}\mathrm{Li}$ are well approximated by an $\alpha + N + N$ three-body model (see, for example, Ref. [54] and references therein), the difference of $J^\pi = 1^-$ and $J^\pi = 0^-$ states of seven-body systems can be essentially caused by the difference of the $\bar{K}NN$ subsystems. Similar to the three-body systems, the level inversion can take place also in the seven-body systems, which is driven by the balance between the nuclear structure and the attraction in the $\bar{K}N$ system.

This property is more pronounced if the strength of the $\bar{K}N$ attraction is further increased. For instance, when we use the AY potential which is more attractive than the Kyoto $\bar{K}N$ potential, the binding energies of ${}^{6}_{\bar{K}}\mathrm{Li}$ and ${}^{6}_{\bar{K}}\mathrm{He}$ with $J^\pi = 0^-$

TABLE VIII. Properties of the ${}^{6}_{\bar{K}}\mathrm{Li}$ system with $J^\pi = 0^-$.

Model	Kyoto		AY
	Type I	Type II	
B (MeV)	69.8	79.7	103
Γ (MeV)	23.7	75.6	88.0
$\delta\sqrt{s}$ (MeV)	$-76.2 - i18.1$	$-15.1 - i10.2$	
P_{K^-}	0.70	0.72	0.64
$P_{\bar{K}^0}$	0.30	0.28	0.36
$\sqrt{\langle r^2_{NN}\rangle}$ (fm)	2.80	2.75	2.57
$\sqrt{\langle r^2_{\bar{K}N}\rangle}$ (fm)	2.52	2.40	2.27
$\sqrt{\langle r^2_{N}\rangle}$ (fm)	1.82	1.78	1.66
$\sqrt{\langle r^2_{\bar{K}}\rangle}$ (fm)	1.61	1.49	1.43
$\langle T\rangle^{K^-}_{G}$ (MeV)	$186 + i19.3$	$213 + i47.9$	$184 + i34.4$
$\langle V\rangle^{K^-}_{G}$ (MeV)	$-220 - i28.5$	$-258 - i69.3$	$-224 - i61.7$
$\langle T\rangle^{\bar{K}^0}_{G}$ (MeV)	$89.5 + i5.08$	$88.9 + i26.5$	$110 + i17.5$
$\langle V\rangle^{\bar{K}^0}_{G}$ (MeV)	$-95.4 - i8.43$	$-97.6 - i33.4$	$-121 - i31.7$
$2\langle V\rangle^{K^-\bar{K}^0}_{G}$ (MeV)	$-30.1 + i0.703$	$-25.6 - i9.55$	$-52.4 - i2.59$
$P^{I=0}_{\bar{K}N}$	0.41	0.41	0.41
$P^{I=1}_{\bar{K}N}$	0.59	0.59	0.59

TABLE IX. Properties of the ${}^{6}_{\bar{K}}\mathrm{He}$ system with $J^\pi = 0^-$.

Model	Kyoto		AY
	Type I	Type II	
B (MeV)	70.6	80.0	103
Γ (MeV)	23.9	75.5	88.0
$\delta\sqrt{s}$ (MeV)	$-75.6 - i18.3$	$-14.9 - i10.2$	
P_{K^-}	0.41	0.41	0.40
$P_{\bar{K}^0}$	0.59	0.59	0.60
$\sqrt{\langle r^2_{NN}\rangle}$ (fm)	2.79	2.74	2.56
$\sqrt{\langle r^2_{\bar{K}N}\rangle}$ (fm)	2.51	2.40	2.27
$\sqrt{\langle r^2_{N}\rangle}$ (fm)	1.81	1.77	1.66
$\sqrt{\langle r^2_{\bar{K}}\rangle}$ (fm)	1.61	1.49	1.43
$\langle T\rangle^{K^-}_{G}$ (MeV)	$115 + i10.5$	$125 + i31.1$	$121 + i21.1$
$\langle V\rangle^{K^-}_{G}$ (MeV)	$-129 - i15.7$	$-144 - i41.5$	$-137 - i37.7$
$\langle T\rangle^{\bar{K}^0}_{G}$ (MeV)	$161 + i14.2$	$177 + i43.4$	$173 + i30.6$
$\langle V\rangle^{\bar{K}^0}_{G}$ (MeV)	$-188 - i21.3$	$-211 - i60.9$	$-208 - i55.4$
$2\langle V\rangle^{K^-\bar{K}^0}_{G}$ (MeV)	$-30.7 + i0.330$	$-26.2 - i9.77$	$-52.8 - i2.72$
$P^{I=0}_{\bar{K}N}$	0.41	0.41	0.40
$P^{I=1}_{\bar{K}N}$	0.59	0.59	0.60

TABLE X. Properties of the ${}^{6}_{\bar{K}}$Li system with $J^\pi = 1^-$.

Model	Kyoto		AY
	Type I	Type II	
B (MeV)	70.8	77.5	92.9
Γ (MeV)	26.4	75.2	88.0
$\delta\sqrt{s}$ (MeV)	$-70.2 - i21.5$	$-13.2 - i10.4$	
P_{K^-}	0.07	0.06	0.16
$P_{\bar{K}^0}$	0.93	0.94	0.84
$\sqrt{\langle r^2_{NN}\rangle}$ (fm)	2.95	2.90	2.83
$\sqrt{\langle r^2_{\bar{K}N}\rangle}$ (fm)	2.54	2.45	2.37
$\sqrt{\langle r^2_{N}\rangle}$ (fm)	1.91	1.88	1.83
$\sqrt{\langle r^2_{\bar{K}}\rangle}$ (fm)	1.54	1.45	1.40
$\langle T\rangle^{K^-}_G$ (MeV)	$33.3 + i5.24$	$27.3 + i16.9$	$57.1 + i8.22$
$\langle V\rangle^{K^-}_G$ (MeV)	$-26.4 - i5.55$	$-21.1 - i16.8$	$-50.3 - i13.7$
$\langle T\rangle^{\bar{K}^0}_G$ (MeV)	$240 + i24.7$	$268 + i61.3$	$219 + i46.1$
$\langle V\rangle^{\bar{K}^0}_G$ (MeV)	$-294 - i35.2$	$-332 - i89.9$	$-275 - i81.3$
$2\langle V\rangle^{K^-\bar{K}^0}_G$ (MeV)	$-23.8 - i2.40$	$-19.2 - i9.03$	$-43.3 - i3.31$
$P^{I=0}_{\bar{K}N}$	0.27	0.27	0.29
$P^{I=1}_{\bar{K}N}$	0.73	0.73	0.71

TABLE XI. Properties of the ${}^{6}_{\bar{K}}$He system with $J^\pi = 1^-$.

Model	Kyoto		AY
	Type I	Type II	
B (MeV)	72.8	80.7	95.6
Γ (MeV)	26.0	75.6	88.5
$\delta\sqrt{s}$ (MeV)	$-71.6 - i20.8$	$-13.8 - i10.4$	
P_{K^-}	0.93	0.94	0.86
$P_{\bar{K}^0}$	0.07	0.06	0.14
$\sqrt{\langle r^2_{NN}\rangle}$ (fm)	2.95	2.89	2.81
$\sqrt{\langle r^2_{\bar{K}N}\rangle}$ (fm)	2.53	2.44	2.36
$\sqrt{\langle r^2_{N}\rangle}$ (fm)	1.91	1.87	1.82
$\sqrt{\langle r^2_{\bar{K}}\rangle}$ (fm)	1.53	1.44	1.39
$\langle T\rangle^{K^-}_G$ (MeV)	$242 + i25.0$	$272 + i61.9$	$223 + i46.8$
$\langle V\rangle^{K^-}_G$ (MeV)	$-298 - i35.9$	$-339 - i91.3$	$-284 - i83.0$
$\langle T\rangle^{\bar{K}^0}_G$ (MeV)	$31.2 + i3.96$	$25.6 + i15.4$	$53.5 + i7.40$
$\langle V\rangle^{\bar{K}^0}_G$ (MeV)	$-24.2 - i4.36$	$-19.7 - i15.2$	$-46.5 - i12.4$
$2\langle V\rangle^{K^-\bar{K}^0}_G$ (MeV)	$-23.3 - i1.69$	$-18.8 - i8.64$	$-42.3 - i3.10$
$P^{I=0}_{\bar{K}N}$	0.27	0.26	0.29
$P^{I=1}_{\bar{K}N}$	0.73	0.74	0.71

become 10 and 7 MeV larger than those with $J^\pi = 1^-$. Namely, the stronger $\bar{K}N$ attraction leads to more drastic level inversion in the seven-body systems. In this way, there is a possibility to extract the information on the $\bar{K}N$ interaction not only from the binding energies but also from the ground state quantum number J^π and from the splitting between $J^\pi = 0^-$ and 1^- states.

Finally, we show, in Figs. 13, 14, 15, and 16, the particle density distributions of the ${}^{6}_{\bar{K}}$He system with $J^\pi = 0^-$ and 1^-. The nucleon density distributions of the ^{6}He ($J^\pi = 0^+$) and ^{6}Li ($J^\pi = 1^+$) systems are also plotted for comparison. In the $\bar{K}NNNNNN$ system with $J^\pi = 0^-$, the central nucleon density becomes slightly larger than that with $J^\pi = 1^-$ and about two times larger than that in the ^{6}Li. Meanwhile, the central antikaon density with $J^\pi = 0^-$ is slightly smaller than that with $J^\pi = 1^-$.

In Fig. 17, we summarize the nucleon and antikaon density distributions of various kaonic nuclei from three- to seven-body systems. The central nucleon densities of the seven-body systems become about half and antikaon densities become one third of the densities of the four- and five-body systems. The central nucleon densities of the five-body systems are highest in the light kaonic nuclei up to seven-body systems, while the densities are not as high as those suggested by using the effective interaction based on the g-matrix approach in Refs. [7,8]. The large nucleon density in the five-body

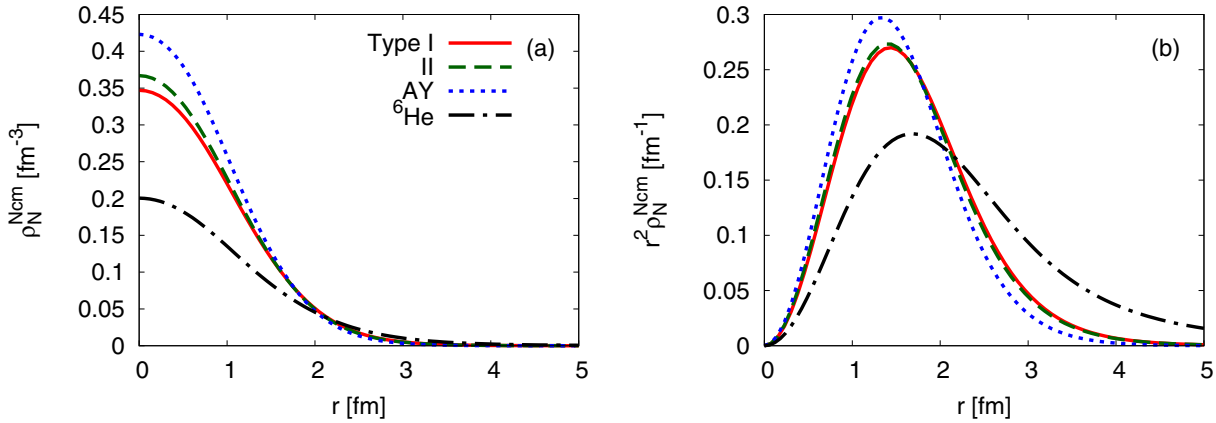

FIG. 13. Same as Fig. 3 but for the ${}^{6}_{\bar{K}}$He system with $J^\pi = 0^-$. The nucleon density distributions for ^{6}He with $J^\pi = 0^+$ is plotted for comparison.

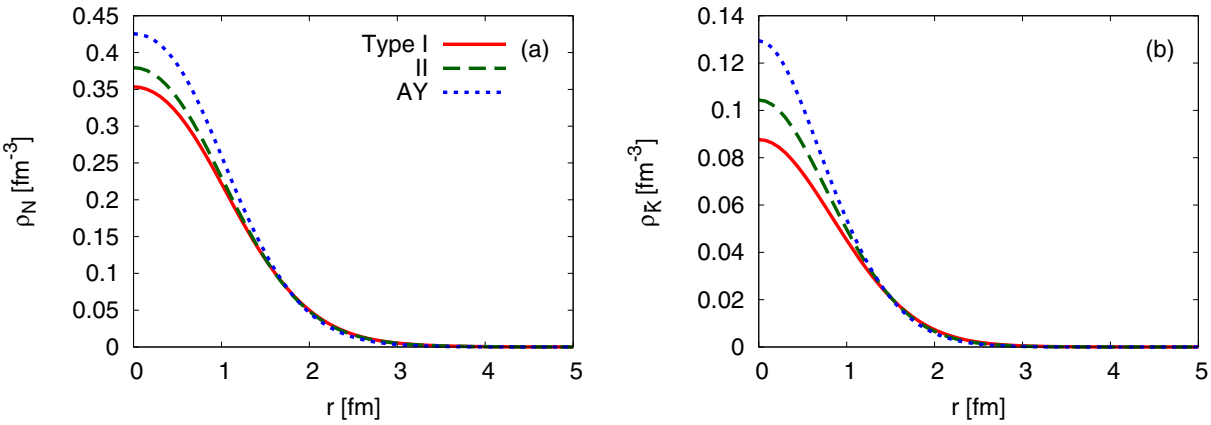

FIG. 14. Same as Fig. 4 but for the ${}^{6}_{\bar{K}}$He system with $J^\pi = 0^-$.

system is mainly caused by the formation of an α-particle configuration, rather than maximizing the $\bar{K}N(I = 0)$ pairs. For the antikaon distribution, the central densities become smaller as the number of nucleons increases. Because the antikaon feels attraction from all the nucleons, its spatial extent increases in a large nucleus.

VI. SUMMARY

We have studied structure of the light kaonic nuclei, $\bar{K}NN$, $\bar{K}NNN$, $\bar{K}NNNN$, and $\bar{K}NNNNNN$ with a powerful few-body approach, the correlated Gaussian (CG) method. Fully converged three- to seven-body solutions are obtained by the stochastic variational method (SVM). As a realistic $\bar{K}N$ interaction, we employ the Kyoto $\bar{K}N$ potential constructed based on the NLO chiral SU(3) dynamics with the SIDDHARTA constraint obtained from Refs. [15,16].

We find one quasibound state in the $\bar{K}NN$, $\bar{K}NNN$, and $\bar{K}NNNN$ systems, and two quasibound states with $J^\pi = 0^-$ and 1^- in the $\bar{K}NNNNNN$ system. All the states are found above the $\pi\Sigma$ emission threshold. The central densities of nucleons are enhanced by an injected antikaon, and become about two times larger than those without an antikaon. The central nucleon density reaches its maximum in the $\bar{K}NNNN$ system with $J^\pi = 0^-$, where the nucleons can form an α-particle configuration. The rms radius of the antikaon increases along with the nucleon rms radius when the mass number is increased.

By decomposing the eigenenergy into different contributions, we find that the K^--$\bar{K}^0$ channel coupling is important for the binding of the light kaonic nuclei. For the $\bar{K}NN$, $\bar{K}NNN$, and $\bar{K}NNNNNN$ with $J^\pi = 0^-$, the core nuclei belong to same isospin multiplet, and the mixing between K^- and $\bar{K}^0$ channels and the energy gains from the off-diagonal components are large. Meanwhile, for the $\bar{K}NNNN$ and $\bar{K}NNNNNN$ with $J^\pi = 1^-$, the channel with core nucleus ^{4}He or ^{6}Li is dominant, and the energy gains from both of the off-diagonal and diagonal components with ^{4}He or ^{6}Li become large.

To take into account the energy dependence of the Kyoto $\bar{K}N$ potential, we examine two methods to determine the $\bar{K}N$ two-body energy in $\mathcal{N}$-body systems (Types I and II). Quantitatively, the binding energies with Type II become gradually larger than those with Type I as the number of particles increase, and the decay widths with Type II become 2–3 times larger than those with Type I. The qualitative features of the kaonic nuclei are not sensitive to the choice of the method.

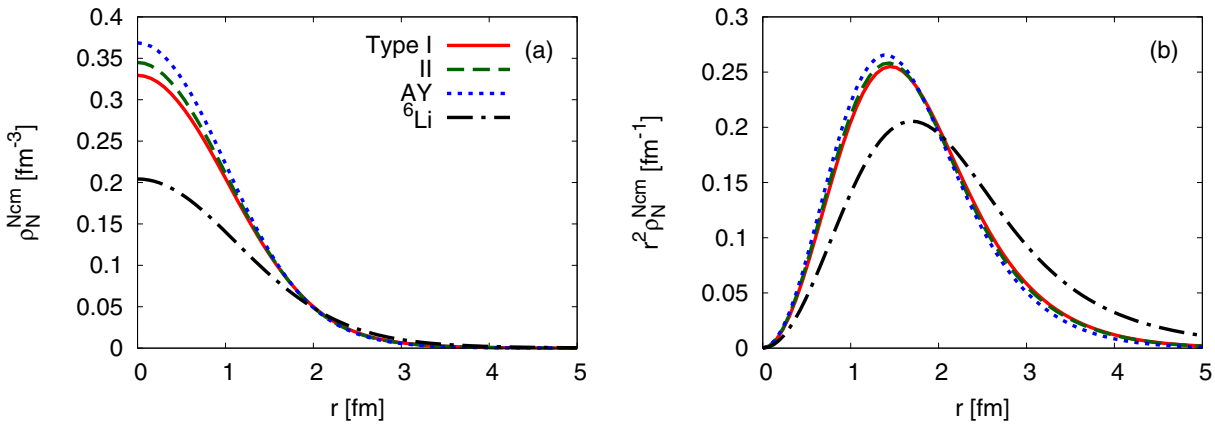

FIG. 15. Same as Fig. 3 but for the ${}^{6}_{\bar{K}}$He system with $J^\pi = 1^-$. The nucleon density distributions for ^{6}Li with $J^\pi = 1^+$ is plotted for comparison.

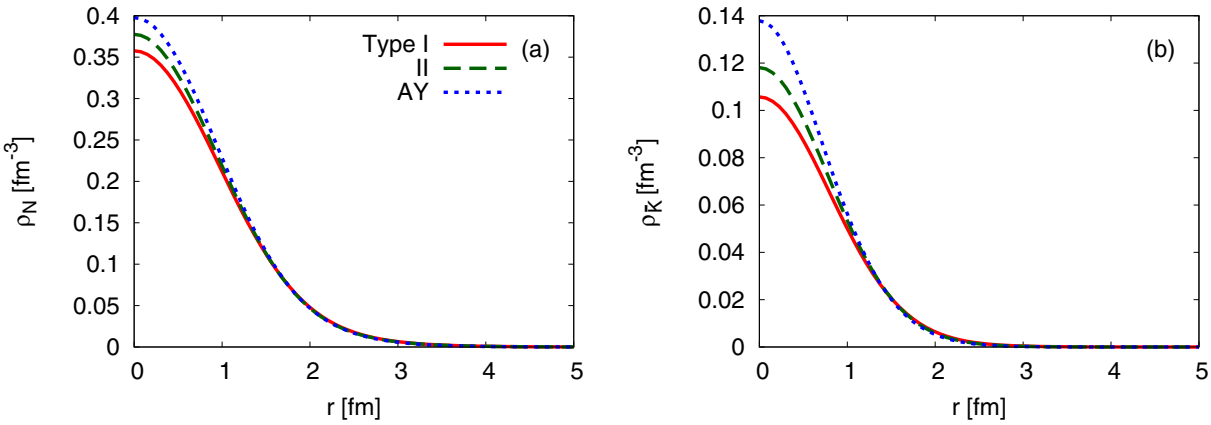

FIG. 16. Same as Fig. 3 but for the ${}^{6}_{\bar{K}}$He system with $J^{\pi} = 1^{-}$.

In order to examine the predictions of deeply bound and high-density kaonic nuclei [4,7,8], we also use the AY potential model. When we employ the AY potential, the binding energies are about 20–30 MeV larger than those with the Kyoto $\bar{K}N$ potential for each system, and decay widths become around 60–80 MeV. Even in this case, the obtained binding energies up to seven-body systems, except $\bar{K}NNNNNN$ with $J^{\pi} = 0^{-}$, are smaller than the 100 MeV predicted by using the optical potential approach [4]. The central density of the $\bar{K}NNNN$ system is not as high as those suggested by using effective $\bar{K}N$ and NN interactions based on the g-matrix approach in Refs. [7,8].

The comparison of the two $\bar{K}N$ potential models (Kyoto $\bar{K}N$ and AY) leads to interesting results in the seven-body systems. If the $\bar{K}N$ attraction is not so strong, we see the spin-triplet ground ($J^{\pi} = 1^{-}$) and the spin-singlet ($J^{\pi} = 0^{-}$) excited states reflecting the lightest core nucleus, ^{6}Li with $J^{\pi} = 1^{+}$. If the $\bar{K}N$ interaction is strong enough as the AY potential, the level ordering of the $J^{\pi} = 0^{-}$ and $J^{\pi} = 1^{-}$ states is inverted. Therefore, it is possible to extract the information on the $\bar{K}N$ interaction from the ground state quantum number J^{π} as well as the energy splitting between $J^{\pi} = 0^{-}$ and 1^{-} of the seven-body kaonic states.

In this work, we employ the single channel $\bar{K}N$ interaction where the $\pi\Sigma$ channel coupling effect is renormalized into its imaginary part. While this potential model reproduces the two-pole structure of $\Lambda(1405)$, we could not find two-pole structure in the kaonic nuclei. One of these poles with the large binding energy and width originated from the $\pi\Sigma$ resonance pole. For the $\bar{K}NN$ three-body systems, the $\pi\Sigma$ channel coupling effect is taken into account explicitly in Refs. [24,29–32], and the two-pole structure is predicted for the energy-dependent $\bar{K}N$ interaction [24]. In order to study the effect of the other pole in the kaonic nuclei, it may be necessary to take into account the channel coupling effect of $\bar{K}N$-$\pi\Sigma$ explicitly.

In addition, we employ the orbital angular momentum independent $\bar{K}N$ interaction, and the hyperon resonances such as $\Sigma(1385)$ except for $\Lambda(1405)$ are not taken into account, although the energy of the kaonic nuclei is close to the threshold of $\Sigma(1385)$ nucleus. However, the coupling effect to the $\Sigma(1385)$ nucleus for these kaonic nuclei is small, as shown in Ref. [23], since we consider the kaonic nuclei with the total angular momentum $L = 0$ where the s-wave $\bar{K}N$ component may become dominant, and $\Sigma(1385)$ is coupled to the p-wave $\bar{K}N$ system. In the case of the kaonic nuclei with total angular momentum $L > 0$, it may be necessary to consider such resonance effects.

ACKNOWLEDGMENTS

The authors thank A. Gal, A. Ohnishi, A. Doté, and Y. Ikeda for helpful comments and discussions. The numerical

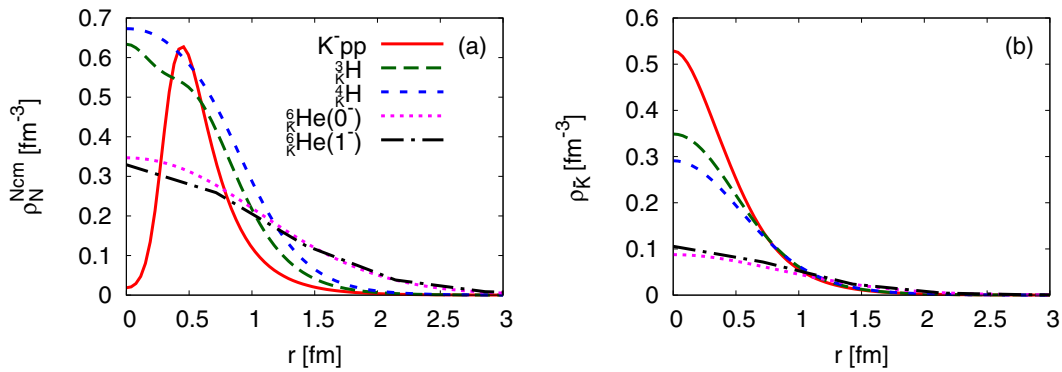

FIG. 17. (a) Nucleon density distributions $\rho_N^{Ncm}(r)$ and (b) antikaon density distributions $\rho_{\bar{K}}(r)$ for the three-, four-, five-, and seven-body kaonic nuclear systems. Kyoto $\bar{K}N$ potential Type I is employed for the $\bar{K}N$ interaction.

calculation has been performed on supercomputers (NEC SX-ACE) at the Research Center for Nuclear Physics, Osaka University and (CRAY XC40) at the Yukawa Institute for Theoretical Physics, Kyoto University. This work was partly supported by the Grants-in-Aid for Scientific Research on Innovative Areas from MEXT (Grant No. 2404:24105008), by JSPS KAKENHI Grant No. JP16K17694, and by the Yukawa International Program for Quark-Hadron Sciences (YIPQS).

[1] C. Patrignani *et al.* (Particle Data Group), Chin. Phys. C **40**, 100001 (2016).
[2] R. Dalitz and S. Tuan, Phys. Rev. Lett. **2**, 425 (1959).
[3] R. Dalitz and S. Tuan, Ann. Phys. (N.Y.) **10**, 307 (1960).
[4] Y. Akaishi and T. Yamazaki, Phys. Rev. C **65**, 044005 (2002).
[5] N. V. Shevchenko, Phys. Rev. C **85**, 034001 (2012).
[6] T. Yamazaki and Y. Akaishi, Phys. Lett. B **535**, 70 (2002).
[7] A. Doté, Y. Akaishi, H. Horiuchi, and T. Yamzaki, Phys. Lett. B **590**, 51 (2004).
[8] A. Doté, H. Horiuchi, Y. Akaishi, and T. Yamazaki, Phys. Rev. C **70**, 044313 (2004).
[9] N. Kaiser, P. Siegel, and W. Weise, Nucl. Phys. A **594**, 325 (1995).
[10] E. Oset and A. Ramos, Nucl. Phys. A **635**, 99 (1998).
[11] J. Oller and U. G. Meissner, Phys. Lett. B **500**, 263 (2001).
[12] T. Hyodo and D. Jido, Prog. Part. Nucl. Phys. **67**, 55 (2012).
[13] Y. Ikeda, T. Hyodo, and W. Weise, Phys. Lett. B **706**, 63 (2011).
[14] Y. Ikeda, T. Hyodo, and W. Weise, Nucl. Phys. A **881**, 98 (2012).
[15] M. Bazzi, G. Beer, L. Bombelli, A. Bragadireanu, M. Cargnelli *et al.*, Phys. Lett. B **704**, 113 (2011).
[16] M. Bazzi, G. Beer, L. Bombelli, A. Bragadireanu, M. Cargnelli *et al.*, Nucl. Phys. A **881**, 88 (2012).
[17] K. Miyahara and T. Hyodo, Phys. Rev. C **93**, 015201 (2016).
[18] T. Hyodo and W. Weise, Phys. Rev. C **77**, 035204 (2008).
[19] D. Jido, J. Oller, E. Oset, A. Ramos, and U. Meissner, Nucl. Phys. C **725**, 181 (2003).
[20] U.-G. Meißner and T. Hyodo, Chin. Phys. C **40**, 100001 (2016), special issue, Review of Particle Physics.
[21] S. Ohnishi, Y. Ikeda, T. Hyodo, and W. Weise, Phys. Rev. C **93**, 025207 (2016).
[22] A. Doté, T. Hyodo, and W. Weise, Nucl. Phys. A **804**, 197 (2008).
[23] A. Doté, T. Hyodo, and W. Weise, Phys. Rev. C **79**, 014003 (2009).
[24] Y. Ikeda, H. Kamano, and T. Sato, Prog. Theor. Phys. **124**, 533 (2010).
[25] N. Barnea, A. Gal, and E. Liverts, Phys. Lett. B **712**, 132 (2012).
[26] A. Doté, T. Inoue, and T. Myo, Prog. Theor. Exp. Phys. **2015**, 043D02 (2015).
[27] T. Yamazaki and Y. Akaishi, Phys. Rev. C **76**, 045201 (2007).
[28] S. Wycech and A. M. Green, Phys. Rev. C **79**, 014001 (2009).
[29] N. V. Shevchenko, A. Gal, and J. Mares, Phys. Rev. Lett. **98**, 082301 (2007).
[30] N. V. Shevchenko, A. Gal, J. Mares, and J. Revai, Phys. Rev. C **76**, 044004 (2007).
[31] Y. Ikeda and T. Sato, Phys. Rev. C **76**, 035203 (2007).
[32] Y. Ikeda and T. Sato, Phys. Rev. C **79**, 035201 (2009).
[33] S. Ohnishi, Y. Ikeda, H. Kamano, and T. Sato, Phys. Rev. C **88**, 025204 (2013).
[34] K. Varga and Y. Suzuki, Phys. Rev. C **52**, 2885 (1995).
[35] K. Varga and Y. Suzuki, Comput. Phys. Commun. **106**, 157 (1997).
[36] Y. Suzuki and K. Varga, *Stochastic Variational Approach to Quantum-Mechanical Few-Body Problems*, Lecture Notes in Physics No. 54 (Springer, Berlin 1998).
[37] N. Hokkyo, Prog. Theor. Phys. **33**, 1116 (1965).
[38] R. B. Wiringa and S. C. Pieper, Phys. Rev. Lett. **89**, 182501 (2002).
[39] G. Audi, A. H. Wapstra, and C. Thibault, Nucl. Phys. A **729**, 337 (2002).
[40] I. Angeli and K. Marinova, At. Data Nucl. Data Tables **99**, 69 (2013).
[41] J. L. Friar, J. Martorell, and D. W. L. Sprung, Phys. Rev. A **56**, 4579 (1997).
[42] A. D. Martin, Nucl. Phys. B **179**, 33 (1981).
[43] T. Sekihara, D. Jido, and Y. Kanada-En'yo, Phys. Rev. C **79**, 062201 (2009).
[44] T. Sekihara, J. Yamagata-Sekihara, D. Jido, and Y. Kanada-En'yo, Phys. Rev. C **86**, 065205 (2012).
[45] M. Bayar and E. Oset, Nucl. Phys. A **883**, 57 (2012).
[46] J. Mitroy, S. Bubin, W. Horiuchi, Y. Suzuki, L. Adamowicz, W. Cencek, K. Szalewicz, J. Komasa, D. Blume, and K. Varga, Rev. Mod. Phys. **85**, 693 (2013).
[47] Y. Sada *et al.* (J-PARC E15 Collaboration), Prog. Theor. Exp. Phys. **2016**, 051D01 (2016).
[48] T. Sekihara, E. Oset, and A. Ramos, Prog. Theor. Exp. Phys. **2016**, 123D03 (2016).
[49] I. R. Afnan and Y. C. Tang, Phys. Rev. **175**, 1337 (1968); Phys. Rev. C **1**, 750(E) (1970).
[50] D. R. Thompson, M. Lemere, and Y. C. Tang, Nucl. Phys. A **286**, 53 (1977).
[51] R. B. Wiringa, V. G. J. Stoks, and R. Schiavilla, Phys. Rev. C **51**, 38 (1995).
[52] Y. Suzuki, W. Horiuchi, M. Orabi, and K. Arai, Few Body Syst. **42**, 33 (2008).
[53] S. Aoyama, K. Arai, Y. Suzuki, P. Descouvemont, and D. Baye, Few Body Syst. **52**, 97 (2012).
[54] W. Horiuchi and Y. Suzuki, Phys. Rev. C **76**, 024311 (2007).